Part III Project Report: Performance studies of ANUBIS detectors

Candidate Number: 8226R

Supervisor: Dr Oleg Brandt

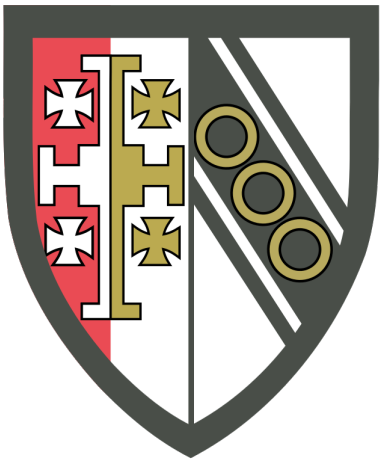

May 13, 2024

Abstract

ANUBIS is a proposed experiment to search for long-lived particles at CERN which could explain Beyond Standard Model phenomena. Understanding the performance of RPC technology is vital for the success of the ANUBIS experiment.

The scintillation counter station in the ATLAS project room is important for acting as a trigger to probe RPC technology. The scintillation counters were upgraded with new components and optimal operating conditions for the scintillation counters to act as a reliable trigger were investigated using threshold voltage scans. When using two scintillation counters in a trigger, a comparator threshold voltage of 720 mV was found to minimise the rate of accidental coincidence between the scintillation counters due to dark counts in the silicon photomultipliers. The efficiencies of the scintillation counters were measured. The efficiency measurements indicated that using a logical OR between silicon photomultipliers in the same scintillation counter, and a trigger threshold voltage of 720 mV, minimised the energy and location bias of the scintillation counter trigger. Efficiencies of 97.2±0.9%, 95.0±0.9% and 93.9±0.8% (within a 95% confidence interval) were found using an OR logic configuration at a threshold voltage of 720 mV.

A track reconstruction algorithm was developed to analyse events from the prototype ANUBIS detector station in CERN. With the LHC beam off, reconstructed tracks had angular distributions that showed agreement with Geant4 simulations of angular distributions of muons from cosmic rays. With the LHC beam on, the prototype ANUBIS detector was shown to have a sensitivity to events produced at the interaction point in the ATLAS experiment. A method for measuring the in-sit efficiencies of RPCs in the ATLAS cavern was developed that minimised the bias effects of using data whose read-out was triggered by the RPCs. The minimum and maximum efficiencies of prototype ANUBIS RPCs measured, at a 95% confidence interval, were 40.8±2.3% and 82.5±2.5%. The in-situ efficiency measurements indicate potential problems with the front-end board electronics or data acquisition system of the prototype ANUBIS setup.

Acknowledgements

I would first like to thank Oleg Brandt for his excellent supervision during the project and for integrating us into discussions of ProANUBIS. The frequent meetings to discuss results helped exponentially. I would also like to thank Aashaq Shah, Michael Revering, Paul Swallow and Giulio Aielli for discussions surrounding ProANUIBS an RPC technology. I'd also like to express my gratitude to Steve Wotton, Richard Shaw and Gaurav Kumar for their help with the scintillation counter and RPC setup in the ATLAS project room. Finally, I would like to thank my fellow Part III students Thomas Adolphus, Peter Wan, Hayden Ramm and Cheetah Zhu for the collaboration, discussions and laughs had during the project work.

Contents

1 Introduction **1**

2 Detector Physics **3**
2.1 Scintillation counters . . . 3
2.2 Resistive plate chambers . . . 4

3 Scintillation counter station **5**
3.1 Overview of the scintillation counter setup . . . 5
3.2 Upgrading the scintillation counter setup . . . 6
3.3 Scintillation counter efficiency measurements . . . 9

4 ProANUBIS reconstruction and data analysis **12**
4.1 Prototype ANUBIS detector . . . 12
4.2 Track reconstruction algorithm . . . 12
4.3 Trajectory timing . . . 16
4.4 Angular distributions . . . 17
4.5 Efficiencies . . . 21

5 Conclusions **23**

A Cosmic rays **24**

B Initial setup tests **25**

C Scintillation Counter calibration and reproducibility **27**
C.1 Calibration . . . 27
C.2 Efficiency measurement uncertainties . . . 28
C.3 Reproducibility . . . 28

D Track reconstruction algorithm **29**

E Angular distributions and detector granularity **31**
E.1 Angles . . . 31
E.2 χ^2 distributions . . . 32
E.3 Detector granularity . . . 32

F ProANUBIS RPC efficiency measurements **33**

References **34**

1 Introduction

The Standard Model (SM) is a theory that describes the fundamental particles of the Universe and their interactions outside of gravity. It has enjoyed significant experimental success, culminating in the discovery of the Higgs boson in 2012 [1].

However, there exist phenomena that cannot be explained by the physics of the SM. Among these is the observation in astrophysics of non-luminescent weakly interacting matter whose existence can only be inferred by gravitational effects, such as is seen in Figure 1. This matter is referred to as "dark matter" (DM) and exists in quantities five times more abundant than normal matter in our Universe.

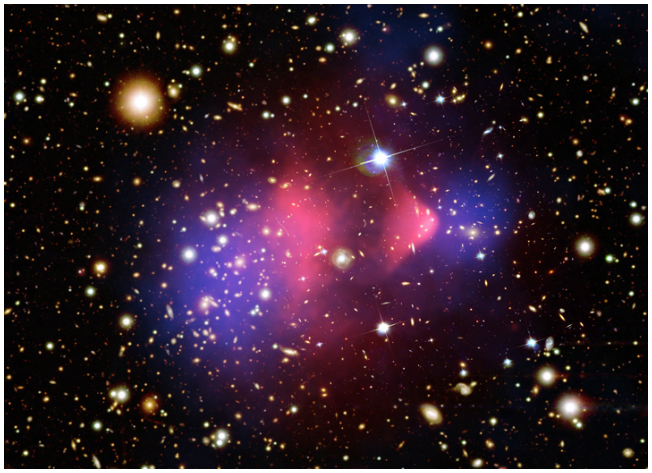

Figure 1: Mass distributions in the "Bullet Cluster", Source: NASA. Direct experimental evidence for DM [2].

Experimental evidence rules out particles in the SM being candidates for DM [3]. Common among theories developed to explain DM, as well as other Beyond SM (BSM) phenomena, is the prediction of long-lived particles (LLPs) [4]. Detection of BSM LLPs in experiments would help to narrow down the list of plausible BSM theories and lead to an improved understanding of the BSM physics sector.

The detection of particles produced in collisions and decays at CERN is achieved by reconstructing their traces in the multiple layers of detectors around an interaction vertex. The particles may then be identified by the energy deposits and tracks they produce during their passage through the detectors. In this context, LLPs refer to particles that decay outside the detection volume of the main detector experiments in CERN, such as ATLAS. To increase CERN's LLP lifetime measurement sensitivity, new detectors capable of detecting products from significantly displaced decay vertices (DDVs) are required [5].

An Underground Belayed In-Shaft Search (ANUBIS) experiment is a proposed particle detector consisting of an array of resistive plate chambers (RPCs) which will be outfitted into the cavern ceiling above the ATLAS detector at CERN, as shown in Figure 2. The addition of ANUBIS at CERN will allow for the detection of LLPs with proper lifetimes (T), $0 < cT/m < 10^6$, a reach increase of 2-3 orders of magnitude compared to currently accepted and running experiments at the LHC [6]. ANUBIS promises comparable LLP lifetime sensitivities to larger scale proposals such as MATHUSLA [7], but by using existing infrastructure in CERN and sharing production run R&D with ATLAS RPC technology, ANUBIS minimises engineering and operational costs.

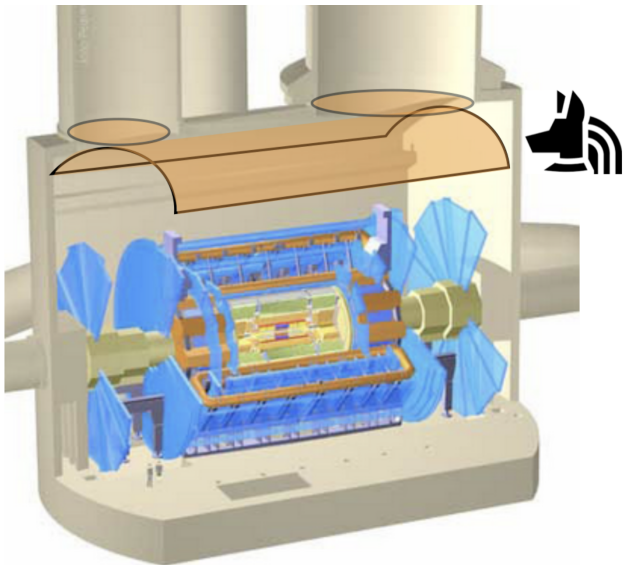

Figure 2: Layout of the proposed ANUBIS array on the ATLAS cavern ceiling, shown in orange [8].

In this project, Peter Wan, Tom Adolphus and I worked on performance studies of RPC technology to be used in ANUBIS. We worked collectively on upgrading the scintillation counter (SC) setup in the ATLAS Project room to be used as a trigger to probe RPCs; testing new BIS-78 gas-gaps and setting up new 50cmx50cm RPC for efficiency measuring. Tom used the setup to measure RPC efficiency with different gas-mixtures and operational parameters. Peter and I worked independently on creating reconstruction algorithms for analysis of prototype ANUBIS data.

2 Detector Physics

2.1 Scintillation counters

Scintillators are materials that exhibit the phenomenon of scintillation, where the scintillator absorbs energy from an incident particle and remits this energy as a photon.

A silicon photomultiplier (SiPM) consists of an array of Si-based photodiodes (PDs) operating in avalanche mode. In a PD, an incident photon of sufficient energy may promote an electron from the valence to conduction energy bands within the depletion region of the PD, creating a photoelectron. If the reverse voltage (RV) applied across the PD exceeds the PD's breakdown voltage, the promoted charge carrier will have sufficient energy to ionise further atoms leading to an avalanche (Figure 3). The recovery time for the bias voltage across the PD determines the measurement rate capabilities of the SiPMs. Thermally excited charge carriers may also generate ionisation avalanches resulting in false particle signals known as "dark counts". The SiPM produces an output voltage in discrete amounts (Figure 4) depending on the numbers of photoelectrons produced.

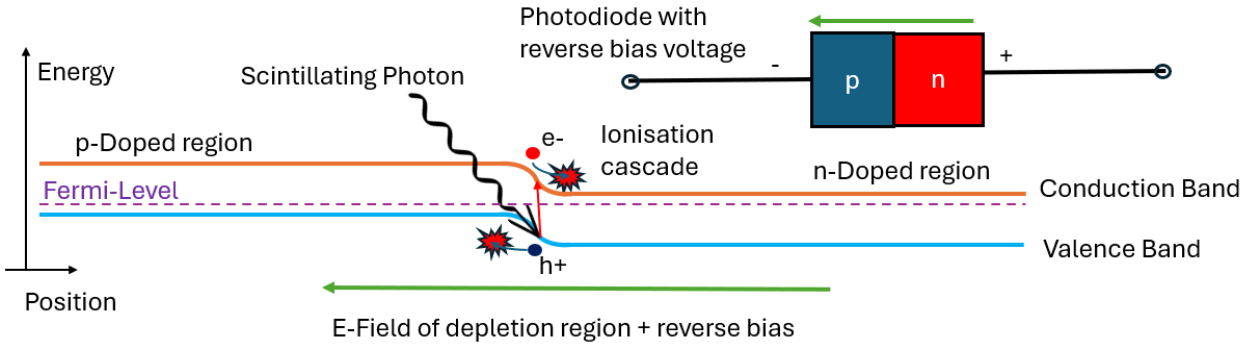

Figure 3: Scintillating photon triggering an ionisation avalanche in the depletion region of the PN junction.

The large movement of charge from the avalanche induces a signal current in detection electrodes as described by the Shockley-Ramo theorem [9]. Signal generation terminates when the charge has reached the electrode. In an SC, the scintillated photon is detected by a coupled PM which converts the light into an electrical signal which is amplified.

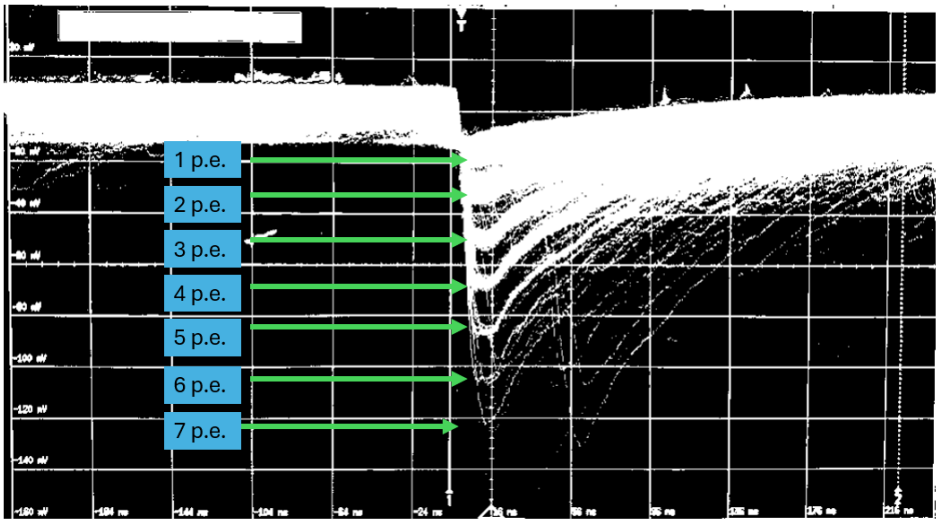

Figure 4: Typical oscilloscope trace of SiPM (SiPM eight here) with the discrete bands due to different number of photoelectrons (p.e.s).

2.2 Resistive plate chambers

Resistive plate chambers (RPCs) are a type of gaseous particle detector. RPCs consist of two parallel plate electrodes made of high resistivity materials, such as bakelite, separated by a gap filled with gas as shown in Figure 5. A high voltage (HV) of order 5 kV is applied across the electrodes.

As a charged particle passes through the RPC gas, it may ionise atoms and molecules inside the gas mixture. Liberated electrons are accelerated by the large electric field and cause further ionisation events in what is known as a Townsend avalanche. The movement of charges in the gas-gap during the Townsend avalanche induces a current into readout strips, as described by the Shockley-Ramo theorem. RPCs offer excellent timing resolution, as there is negligible drift time for the ionised electron before avalanche formation.

An RPC is said to operate in streamer mode if the formation of the Townsend avalanche is aided by photo-ionisation [10]. For our performance studies, the transition to streamer mode in the RPCs is unwanted as streamers introduce large discharges on the electrodes which increases recharge time and reduces rate capability. The large discharge can also lead to large currents that damage front-end board (FEB) electronics. The transition from avalanche mode to streamer mode is suppressed by using a quenching gas which absorbs the wavelength of photons that would cause photo-ionisation.

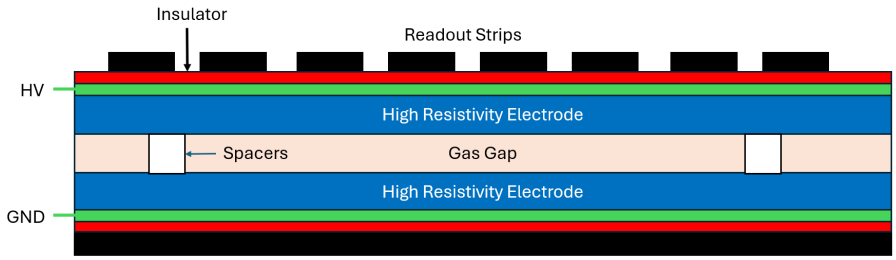

Figure 5: Cross section of a typical RPC.

3 Scintillation counter station

3.1 Overview of the scintillation counter setup

The SC station (Figure 6) consists of three SCs each containing a 50cm×50cm×1cm volume of EJ-200 scintillating material with two AFBR-S4N33C013 Broadcom SiPMs placed at 45° on the corners of one face of the scintillator [11]. The SC station is used as a trigger to probe RPCs.

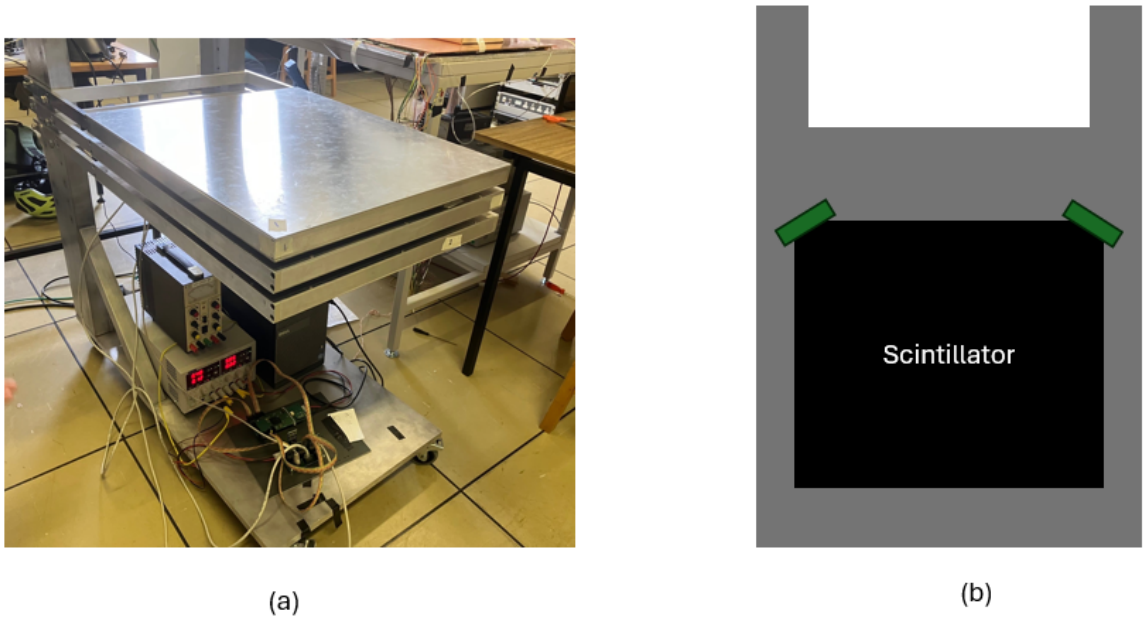

Figure 6: (a) The SC trolley in the ATLAS project room. (b) Schematic of the inside of each tray on the SC trolley. The two SiPMs are shown in green.

Without a particle source, this project relied on muons produced from cosmic rays (discussed in Appendix A). The expected muon arrival rate for detectors in this project is of the order 10-100 Hz, considering the dimensions of detectors used and cosmic muon flux of 1 cm^{-2} min^{-1} for horizontal detectors [12]. After scintillation, EJ-200 has a dead time of 3 ns during which new particles cannot trigger an emission pulse [13]. The EJ-200 scintillator's sampling rate capability is completely adequate for sampling muons of cosmic ray origin, and there is no risk of aliasing. The Broadcom SiPMs have a recovery time of order 60 ns [14], giving them a rate capability of the order of 10s of MHz and making them appropriate to measure scintillating photons resulting from cosmic ray muons. The photon detection efficiency (PDE) of a SiPM is the proportion of photons which pass through the SiPM and result in a detection. The Broadcom SiPMs used have a peak PDE at wavelengths around 425 nm, which corresponds to the wavelength at the peak of the EJ-200 emission spectrum [13, 14]. This maximises the probability of particle detection by the SC system.

The principal electronic components of the SC station are the comparators, VBIAS generators and the field-programmable gate array (FPGA) coincidence board. The comparators compare the voltage produced by the SiPMs with some threshold voltage set by software and decide what signals to send to the FPGA, with smaller threshold voltages requiring more pho-

toelectrons for signal passage. This is important for filtering out dark counts, which tend to produce voltages corresponding to one or two photoelectrons and rarely more due to optical crosstalk [15]. The VBIAS generator supplies the RV necessary for avalanche mode operation of PDs in SiPMs. The FPGA decides if signals from the comparators are coincident in a 10 ns time window, in logic set by the user. The FPGA interfaces with TBtrigger software, where counts are logged. The FPGA has five channels: A, B, C, D and E for six SiPMs. Channel E is a logical OR of two SiPMs.

3.2 Upgrading the scintillation counter setup

Threshold voltage scans of the dark count rates (DCRs) of the initial setup's SiPMs were performed (Appendix B). TBtrigger was used to change the comparator threshold voltage and log counts. Issues of noise and SiPMs not working were found, as noted by students previously [16]. New comparator and VBIAS generator boards were assembled. A power distribution board (PDB) was created to supply the necessary voltages to the various boards. New flexible SiPM PCBs and SiPM mounts were implemented into the setup and connected to the PDB with RJ-45 connectors (Figure 7). The new VBIAS generator board outputs 30 V RV across the SiPMs.

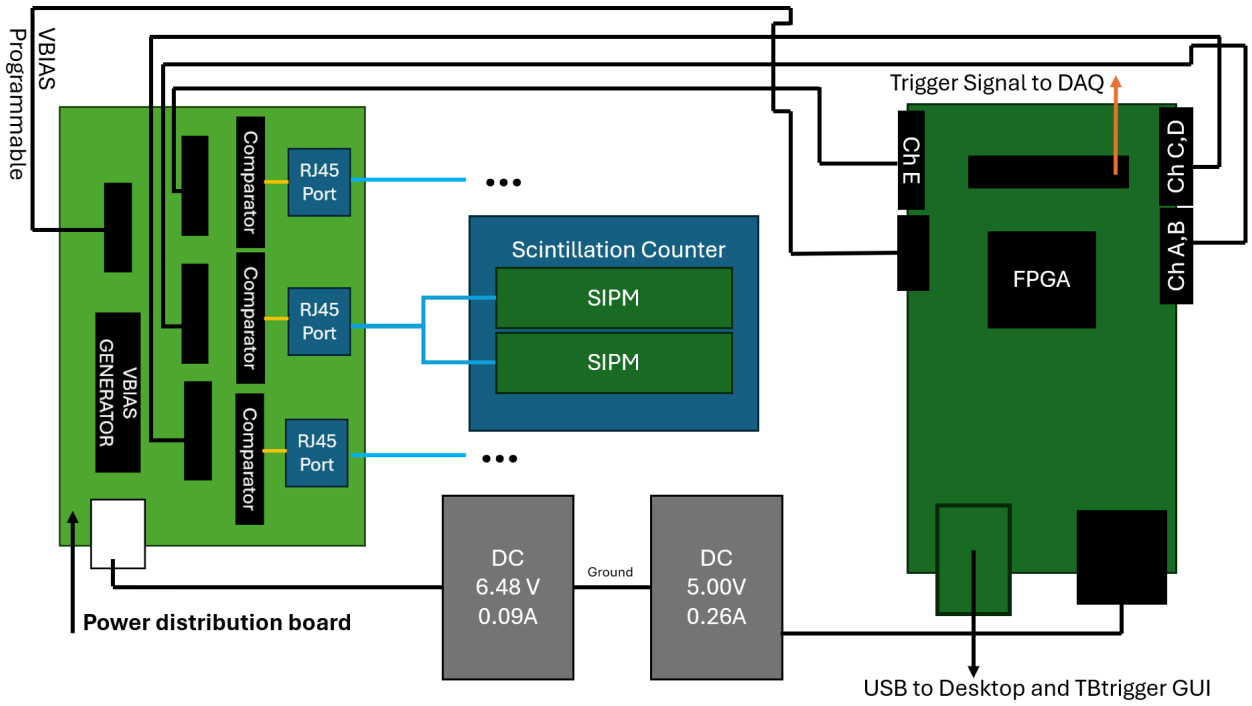

Figure 7: New SC setup.

To verify the new setup was functioning, threshold voltage scans of SiPM count rates in SCs were measured. Figure 8 shows threshold scans for SiPM eight using different comparator channels. The sources of error in threshold scans were shot noise and time resolution (Appendix B), both minimised by recording points for at least one minute each. The expected step structure is resolved using 2 mV increments in threshold voltage. Each step corresponds to changing the number of photoelectrons in a signal by one. The drop in hit rate for threshold voltages above 770 mV is due to saturation of electronics by dark-counts. It was found that different

comparators produced different threshold voltage scans for the same SiPM. This effect may be explained by the tolerance of components on the comparator board. The comparators were calibrated for these offsets (Appendix C.1). Discrete bands were observed in the oscilloscope traces of the new SiPMs (Figure 4).

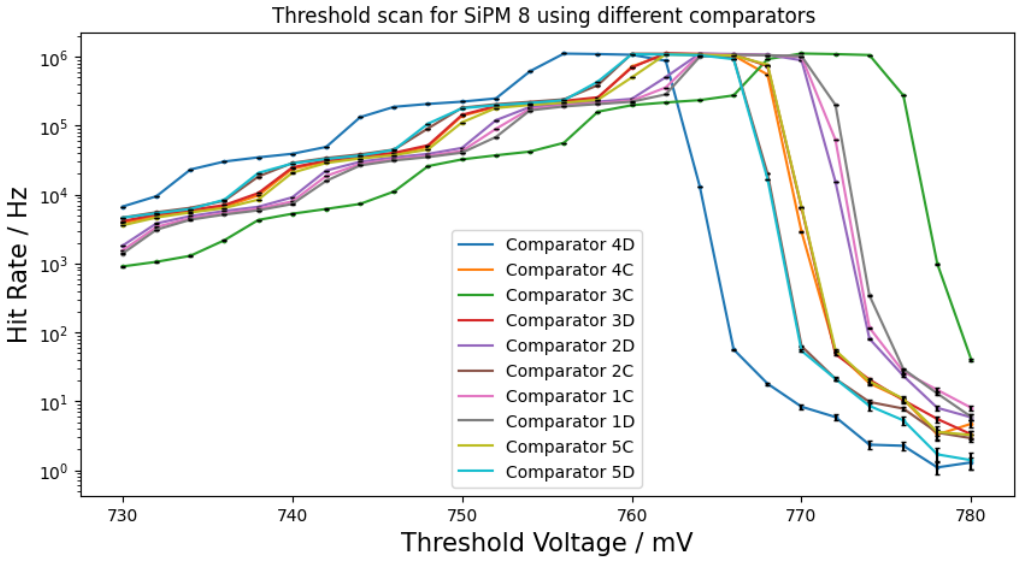

Figure 8: Threshold scan for SiPM eight using different comparators.

Threshold scans of the rate of a logical AND (&&) between two pairs of two SiPMs in a logical OR (||) were performed with varying separations between the scintillators. Figure 9 shows two regimes in this threshold scan. DCR does not depend on the separation of scintillators and dominates the coincidence counts measured above a threshold voltage of 730 mV. Below 730 mV, the count rate decreases with increased separation. This effect is explained as reducing the solid angle possible for muons to traverse both detectors.

Next, the SCs were horizontally displaced to minimise the chance a single muon could pass through two or more at once. The rate of "accidental coincidence" between the SCs was then measured. The rates were found to plateau (Figure 10), suggesting a large number of photoelectrons are produced concurrently. As the scintillators are separated by around a metre, the plateau suggests a number of particles with correlated arrival times over a spread-out area. A possible explanation is multiple particles from a cosmic ray air shower (Appendix A).

For the SCs to be good triggers for testing the RPC, the threshold voltage chosen must reliably trigger on real particles and not dark counts. A threshold voltage of 720 mV was chosen for the SC trigger. This threshold voltage is at the beginning of the plateau for the trigger logic (A||B)&&(C||D) in Figure 10 where the "accidental coincidence" is dominated by real particles and not coincident dark counts, so there is a negligible background to subtract from measurements. Muons from cosmic rays have an average energy of 4 GeV [12] at Earth's surface. Their average energy loss per distance traversed through matter is well-modelled by the Bethe-Bloch formula (Appendix A) and is proportional to the distance travelled through matter. Using a lower threshold voltage would require more photoelectrons to trigger a signal, which would bias for muons with longer path lengths through the scintillators.

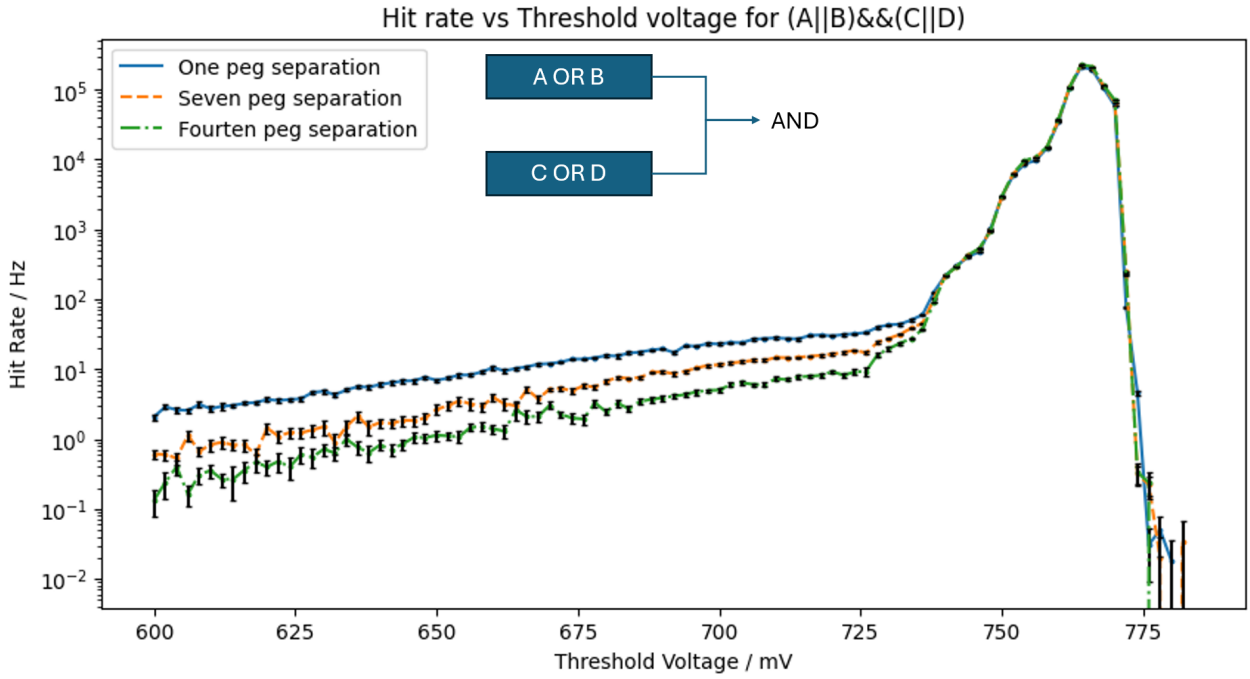

Figure 9: Threshold scan with varying separation between scintillators. One peg separation is 5 cm.

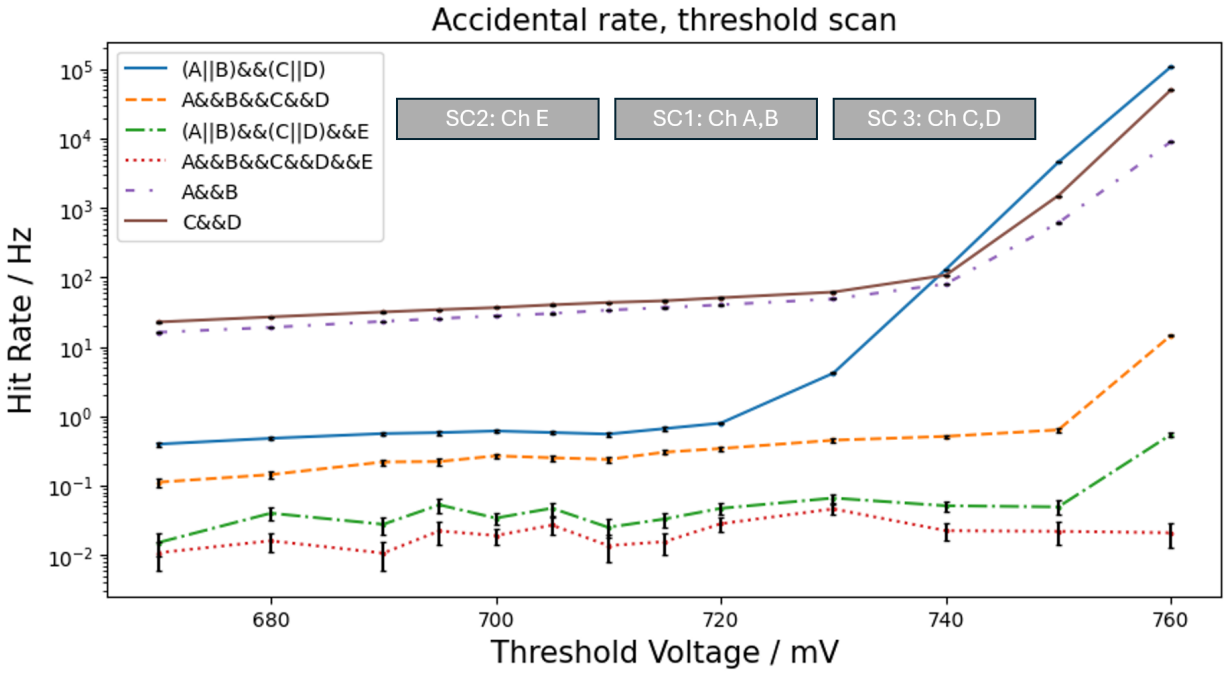

Figure 10: Coincidence rate of three horizontally separated SCs, with different logic configurations.

3.3 Scintillation counter efficiency measurements

The detection efficiency, η, of each SC was measured by using the other two SCs as a trigger in the configuration shown in Figure 11. The threshold voltage of the trigger SCs was fixed at 720 mV, based on discussions in 3.2.

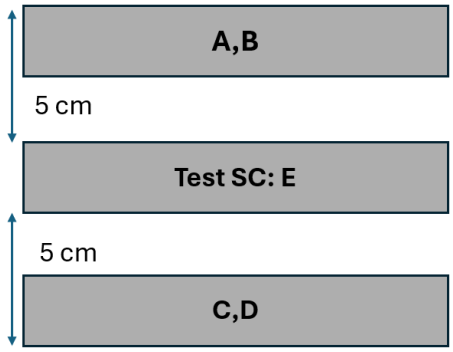

$$\eta_{OR} = \frac{(A\|B)\&\&(C\|D)\&\&E}{(A\|B)\&\&(C\|D)} \quad (1)$$

$$\eta_{AND} = \frac{(A\&\&B)\&\&(C\&\&D)\&\&E}{(A\&\&B)\&\&(C\&\&D)} \quad (2)$$

Figure 11: Setup for measuring efficiency of test SC.

Threshold voltage scans of the efficiencies of the SCs in OR and AND logic configurations, defined by equations (1) and (2) respectively, were performed. Efficiencies of 93.9±0.8%, 97.2±0.9% and 95.0±0.9% were measured at 720 mV (Figure 12). This is an improvement on the peak efficiency of 70% measured with the previous setup [16]. The uncertainties are for 95% confidence intervals and are discussed in Appendix C along with the reproducibility of the results in Figure 12 when the comparator offsets are accounted for. No background counts were subtracted, for reasons discussed in Section 3.2.

Decreasing the threshold voltage increases the number of photoelectrons required to detect a particle. This leads to a drop in efficiency due to the limited PDE and finite area of the SiPMs. The efficiencies for the SCs in the AND configuration drop off faster with decreasing threshold voltage compared with the OR configuration. The AND configuration biases for muons passing through the SCs at points roughly equidistant from the SiPMs (Figure 13(b)). The geometry then biases for muons with shorter path lengths, which deposit less energy and are less likely to be picked up by the SiPMs of the test SC.

It is important to minimise the location and energy bias of the SC trigger so that it can probe the entire RPC area with a large dynamic range of energies. The OR configuration exhibits no bias for any location in the scintillator, as a muon can hit on either side and cause a trigger (Figure 13(a)). A 720 mV trigger threshold voltage was chosen as it maximises the muon trigger rate with negligible accidental DCR background. Decreasing the threshold voltage biases for muons passing closer to the SiPMs (Figure 13), as the solid angle of the SiPMs seen by photons is larger there. To improve, three SCs in a trigger would allow for the threshold voltage to be increased while keeping the accidental rate low.

The SC trigger setup was then used to probe new 50cm×50cm RPCs we constructed from new gas-gaps we tested.

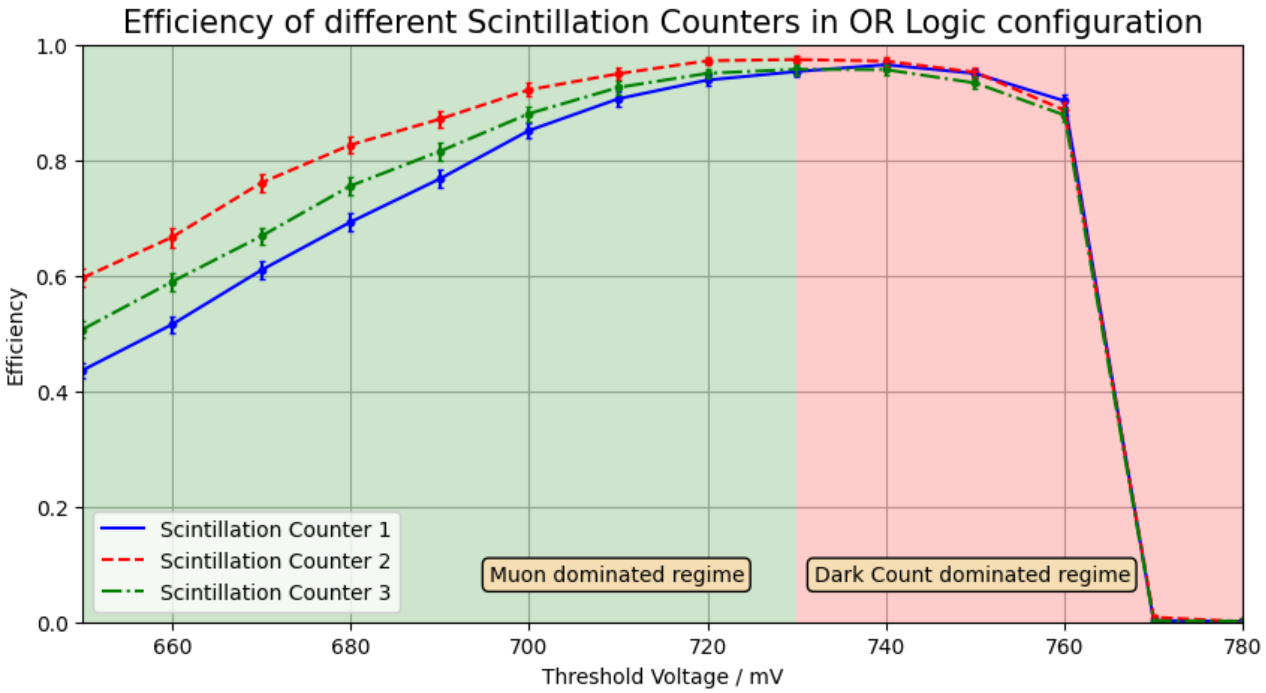

(a)

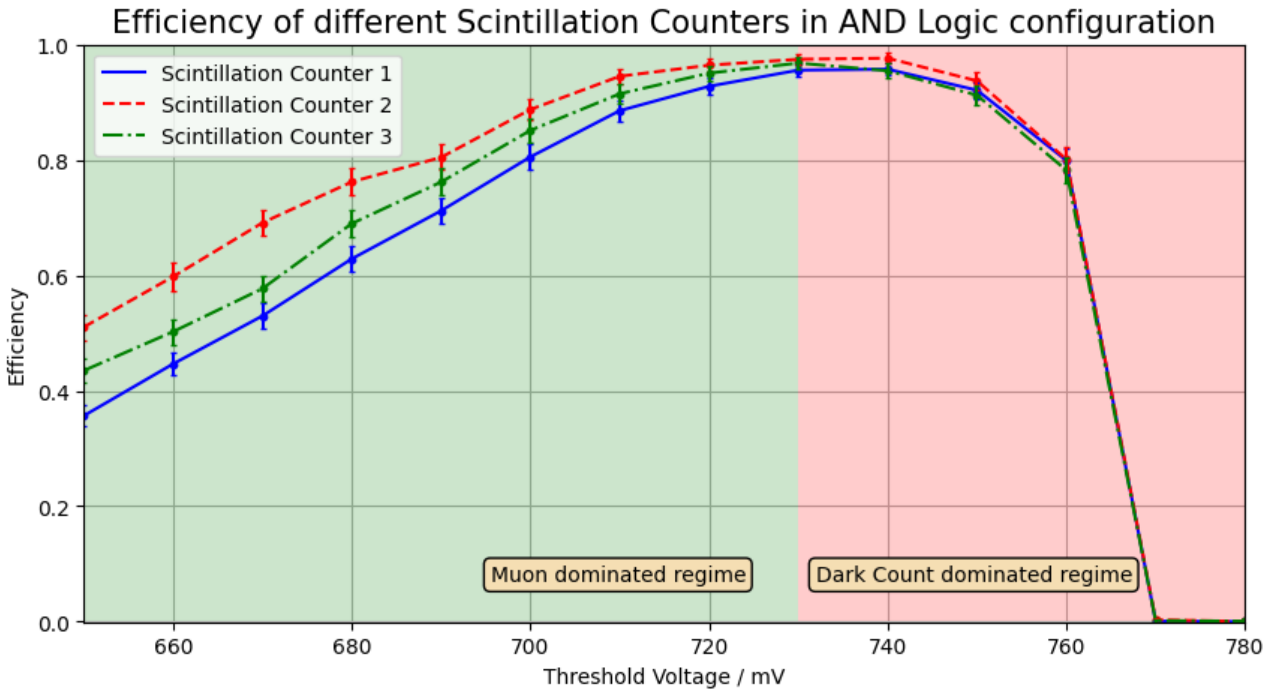

(b)

Figure 12: SC efficiency scan using (a) (A||B)&&(C||D)&&E logic and (b) A&&B&&C&&D&&E logic.

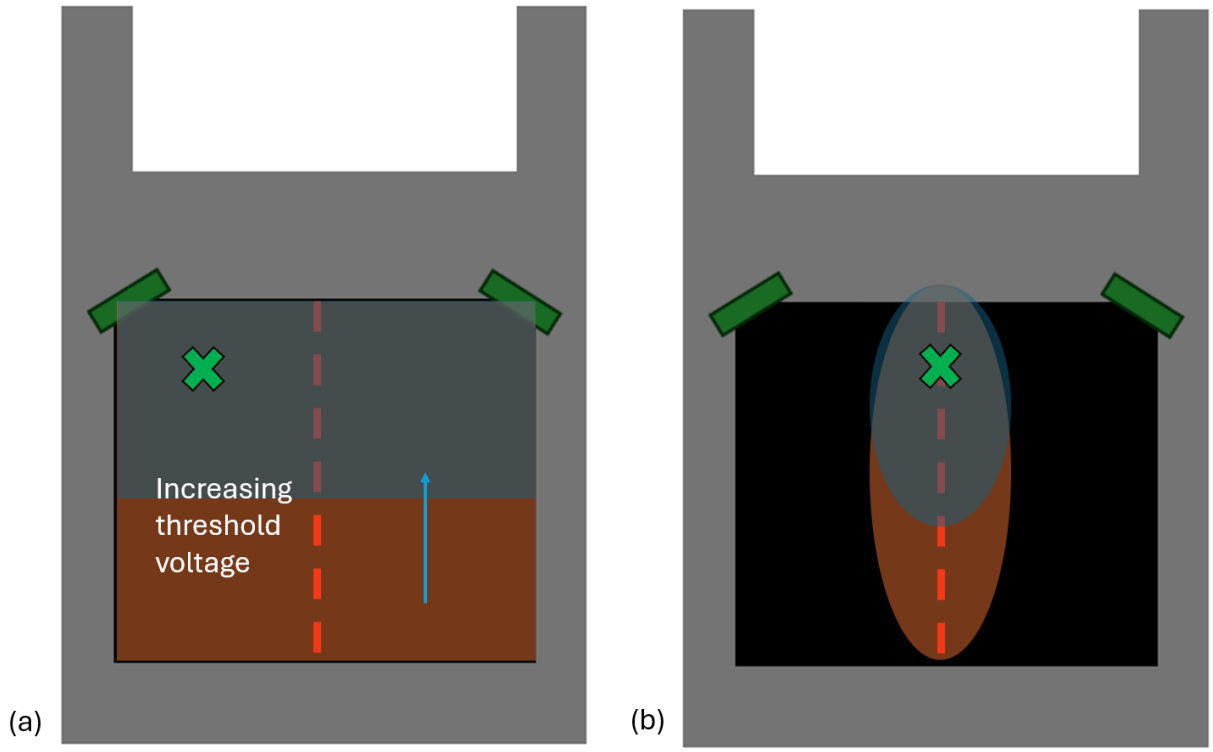

Figure 13: Inside of SC tray, the red line is the locus of points equidistant from both SiPMs. (a) The OR configuration has no bias for location. (b) The AND configuration biases for locations nearly equidistant from both SiPMs.

4 ProANUBIS reconstruction and data analysis

4.1 Prototype ANUBIS detector

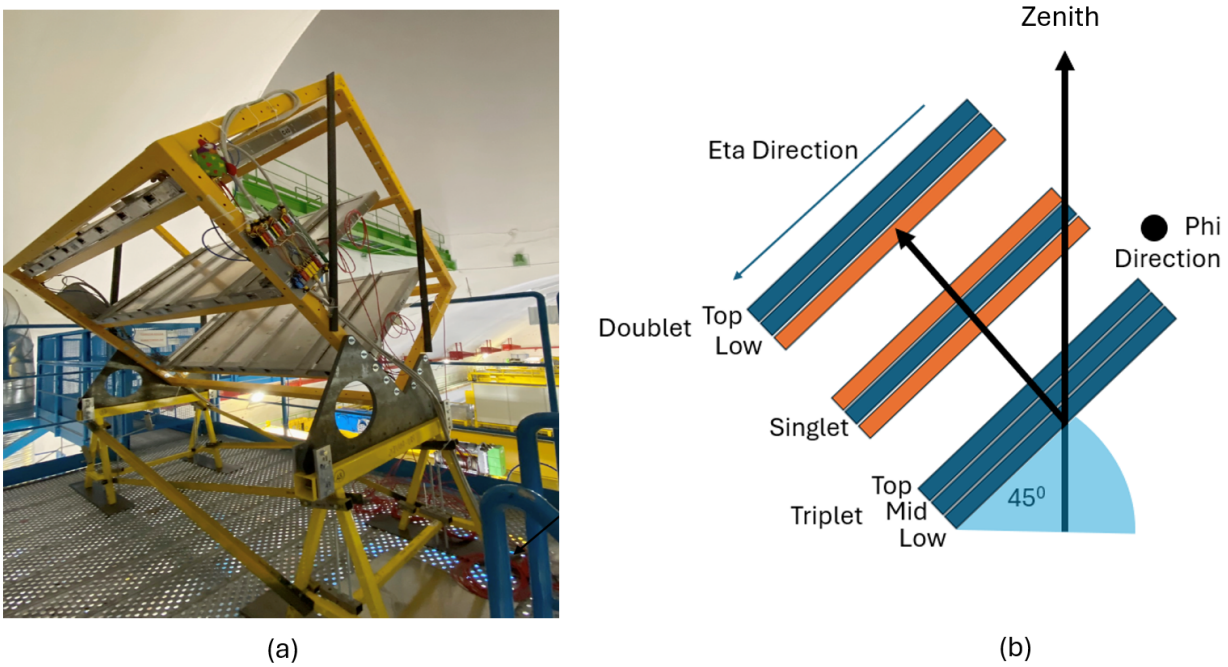

Figure 14: (a) Image of ProANUBIS setup in the ATLAS cavern. (b) Schematic of ProANUBIS RPC triplet, singlet and doublet configuration. The blue volumes are occupied by RPCs and the orange volumes are not.

A prototype detector "ProANUBIS" has been set up facing the interaction vertex in the ATLAS cavern [17], consisting of three chambers of BIS-78 RPCs arranged in a triplet, singlet and doublet fashion (Figure 14(b)). Each RPC consists of 64 and 32 channels in the phi and eta directions respectively.

ProANUBIS allows for validation of current and future simulations of backgrounds ANUBIS will encounter. The largest anticipated backgrounds are cosmic ray muons, long-lived neutral kaons (K_L^0) decays and production of jets from K_L^0 or neutron (n^0) interactions with air molecules [18]. It is anticipated the ATLAS detector will act as a passive shield and veto for n^0 and K_L^0 backgrounds [18, 19], while the rock above the ATLAS cavern will act as a shield for cosmic muons. The cosmic muon background can be filtered by using the direction of reconstructed particle tracks in ProANUBIS, reliant on the timing precision of the RPCs explored here.

ProANUBIS allows for assessment of BIS-78 RPC capabilities and insights into engineering challenges facing the construction of the ANUBIS detectors, including civil engineering problems and data acquisition (DAQ) implementation and readout [17].

4.2 Track reconstruction algorithm

Accurate placement of DDVs is necessary for particle identification of LLPs, in a process similar to b-tagging [20]. The track reconstruction algorithm is important for this identification process

and for filtering backgrounds.

A track reconstruction algorithm was developed to reconstruct the trajectories of particles passing through ProANUBUIS. See Appendix D for a detailed description. The current DAQ implementation triggers a readout whenever three eta channel hits are coincident within 60 ns. The readout then contains data of times phi and eta channels fired in each RPC over 1.25 μs after the trigger. When a real particle passes through ProANUBIS, the hit times of RPC channels are correlated and occur close together.

The reconstruction algorithm first clusters data in time using an adaptive time windowing. Following temporal clustering, channel strips are grouped spatially into clusters, defined as a continuous block of channels hit within a time window. Coordinates of hits are then determined by the mid-points of these clusters. This procedure can result in multiple (x,y) coordinate pairs for each RPC (Figure 15). Every possible combination of (x,y) coordinates across the RPCs is then determined. A filter is then applied to possible events, based on the number of RPCs and/or the number of chambers involved.

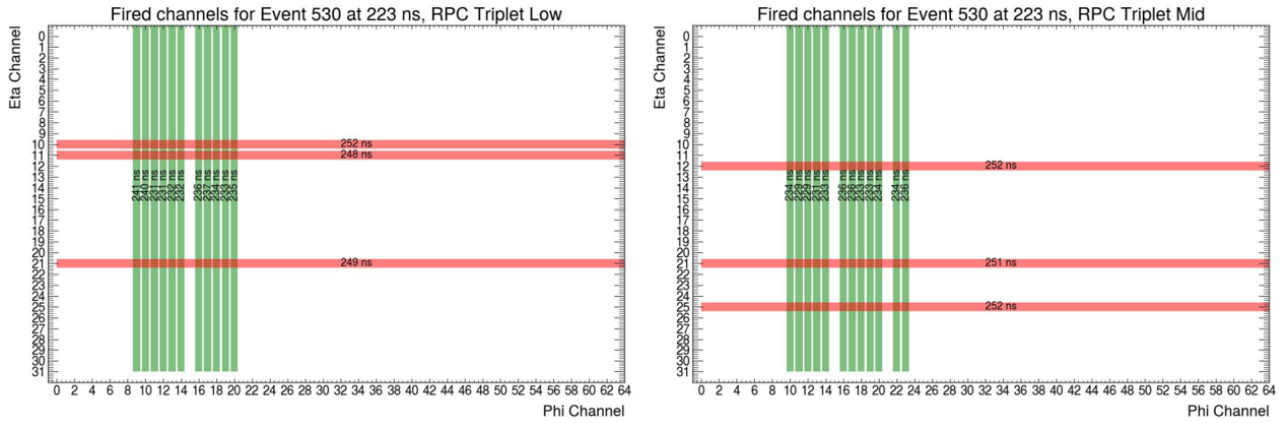

Figure 15: Example event display of a cosmic muon passing through two RPCs in the triplet chamber. The clusters can be seen as the continuous blocks of channels. Where eta and phi channel hits intersect, a possible (x,y) coordinate pair is produced.

ProANUBIS is not situated in any large magnetic fields, so the expected particle trajectories are straight lines and the usual method of Kalman filtering used for curved track fitting [21] is not necessary here. Instead, singular value decomposition (SVD) is used to fit a straight line through each possible combination of coordinates generated. SVD determines the direction vector of a line, passing through the geometrical mean of the coordinates, which minimises the total perpendicular squared distance of the coordinates from the line [22]. χ^2 values, normalised by the number of degrees of freedom in the fit, are then calculated for each fitted combination. The track that has the minimum normalised χ^2 value is selected as the best track. Examples of fitted events are shown in Figure 16.

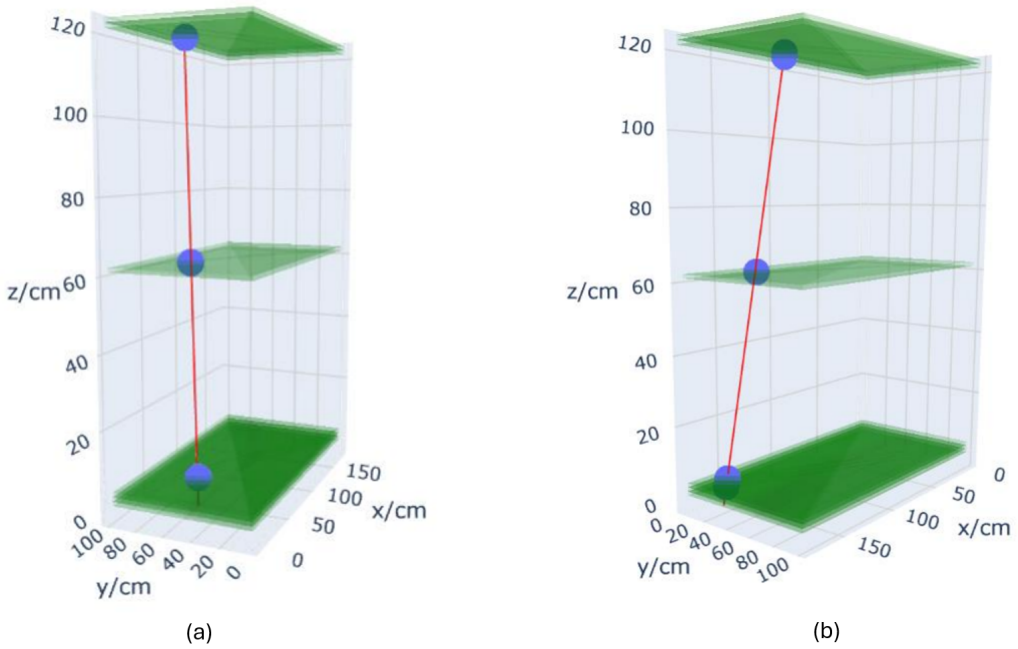

Figure 16: The red line shows the reconstructed track, the green shapes are the RPCs and blue dots are the locations of hits. (a) Example event during ATLAS luminosity spike. (b) Example event while the LHC beam was off.

The errors in the x and y coordinates are assumed to originate from a uniform distribution of the size of one strip width in the phi and eta directions respectively. These errors are used in the weighting of χ^2 values for x and y independently, which are then summed. Figure 17 shows the normalised χ^2 distribution for tracks detected by at least five RPCs. The distribution shape matches one expected for a normalised χ^2 distribution with more than two degrees of freedom. The peak of slightly less than one would indicate errors in coordinates are being overestimated. Figure 18(a) shows the normalised χ^2 distributions for tracks with at least four RPCs. The number of degrees of freedom in this case is at least four (at least eight coordinates with four fitting parameters), so a peak at zero is not expected. Figure 18(b) shows that the peak at zero normalised χ^2 is diminished if a requirement on the track to have a hit in all three chambers is included. This implies the peak at zero is an artifact of the detector setup, with the singlet and doublet having long lever arms to drag reconstructed tracks if one but not the other is present.

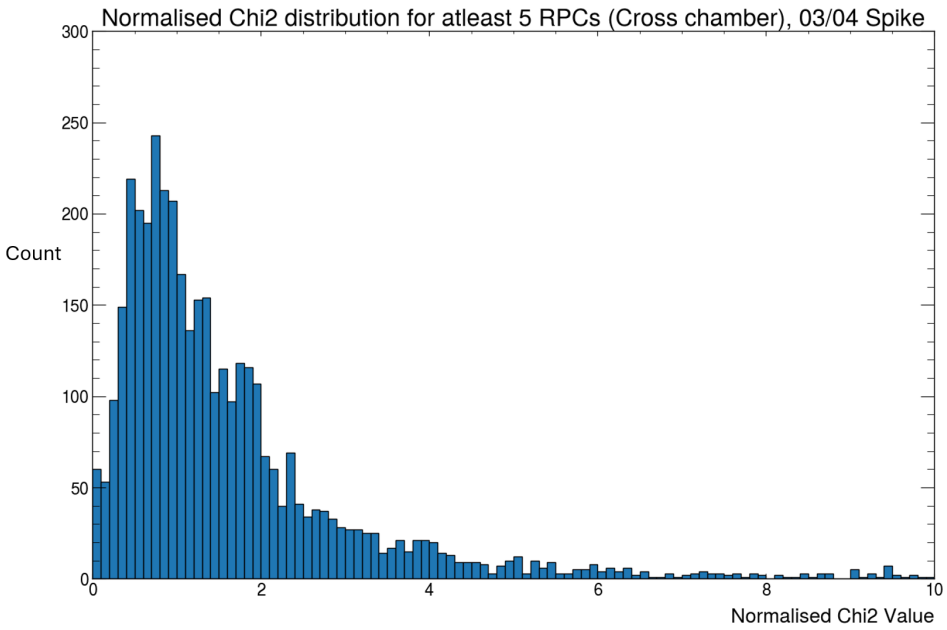

Figure 17: Normalised χ^2 distribution for tracks reconstructed with at least five RPCs, with the LHC beam on.

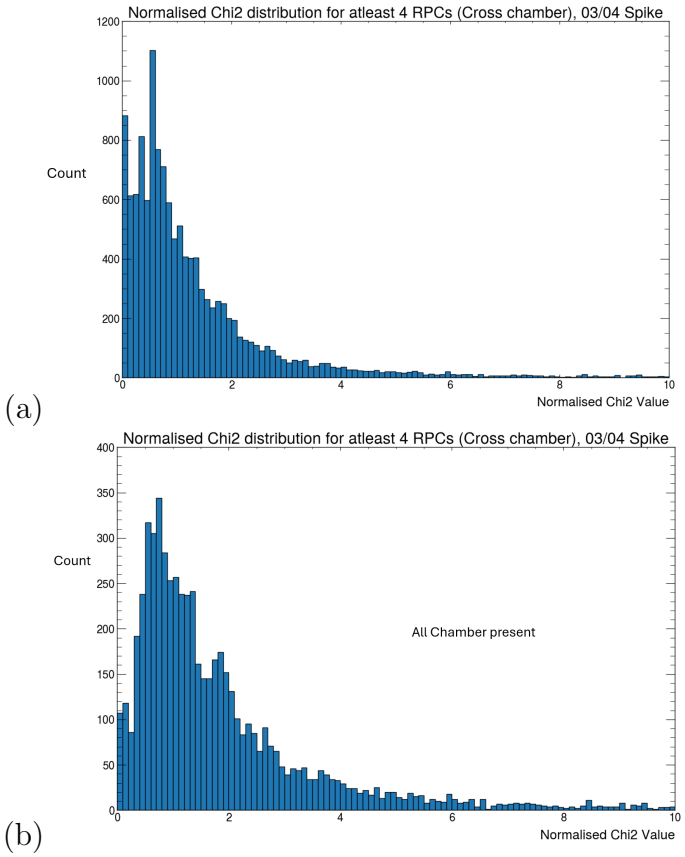

Figure 18: Normalised χ^2 distribution for tracks reconstructed with at least four RPCs, with the LHC beam on, without (a) and with (b) constraint on all chambers being present.

Events were initially reconstructed using an adaptive time window of 15 ns, with a normalised χ^2 cut-off of 10 to avoid bad reconstructions. The height of ProANUBIS is approximately 1.2 m, so for particles travelling near c a traversal time of around 4 ns would be expected. The 15 ns time window was chosen to allow for uncertainties due to signal propagation time in channels, known as "time-walk", and the effect of different FEBs and time to digital converters (TDCs). Figure 19 shows the distribution of cluster sizes seen by ProANUBIS, a max cluster size of three was chosen for reconstructions. Previous performance studies of RPCs at ATLAS found the average cluster size for cosmic muons was between one and three [23].

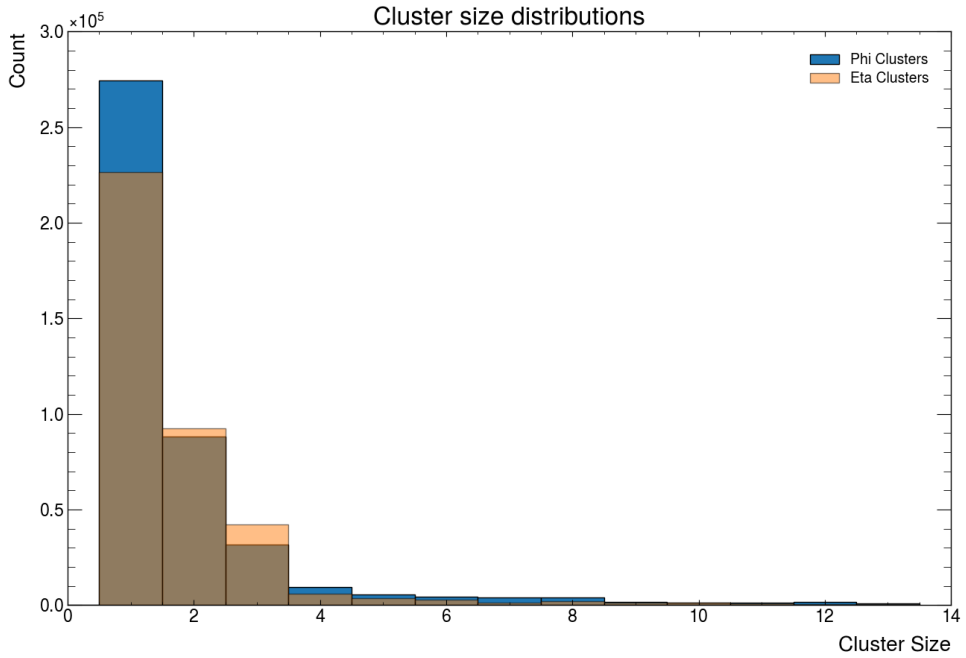

Figure 19: Cluster size distribution for ProANUBIS RPCs.

4.3 Trajectory timing

The direction of reconstructed tracks is determined by the timing of hits in RPCs. The ability to distinguish between vertically upward or downward travelling particles is required for ANUBIS detectors to filter out cosmic muon backgrounds. The algorithm uses differences in phi hit times, averaged over their clusters, for the top-most hit RPC compared to the bottom-most hit RPC (dT). The phi channels were chosen since they are shorter and less affected by time-walk effects.

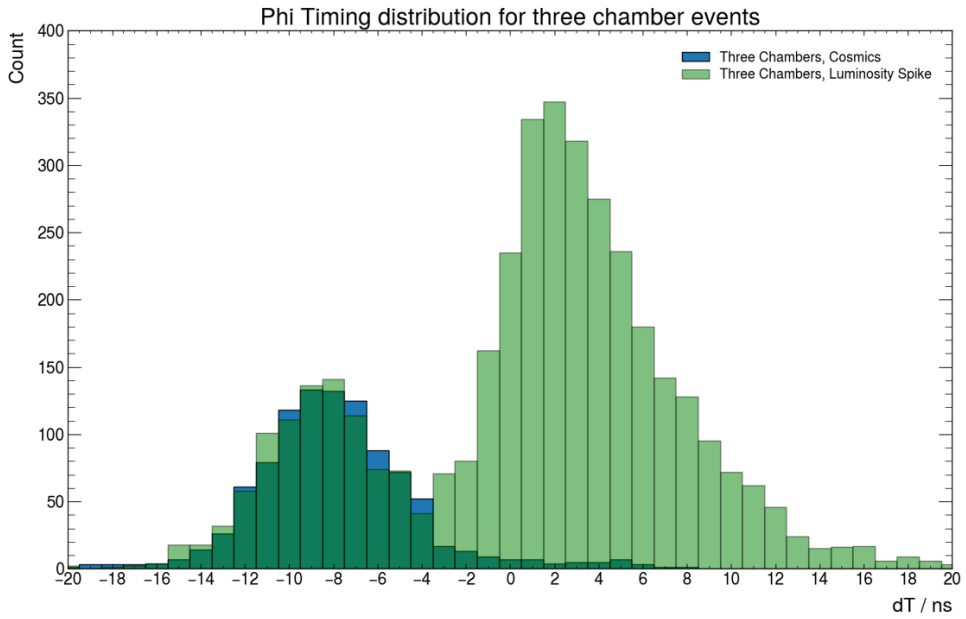

Figure 20: dT distribution, both with the LHC beam on (green) and off (blue).

Figure 20 shows the distribution of event timings for cross-chamber events, with the LHC beam on and off. Given a vertical height of 1.2 m, events are expected to peak at $\pm$ 4 ns for particles travelling near c. ProANUBIS shows a good ability to filter cosmic muons using trajectory timings. However, Figure 20 suggests there are misidentification of track trajectories caused by a convolution of lots of errors. A breakdown of timing offsets for different FEBs and TDC chips should be carried out. The time-walk of signals along read-out strips should be accounted for and a new metric for determining the hit times of clusters should also be investigated, such as the earliest hit time in a cluster as suggested in previous performance studies [23].

4.4 Angular distributions

The angular distributions of reconstructed tracks were investigated to see if the reconstruction algorithm could be validated by physical simulations. The definition of angles studied, as well as the χ^2 distributions of reconstructed events, are detailed in Appendix E.

Geant4 simulations, considering the geometry of the ATLAS cavern and shaft and energy losses of cosmic muons traversing through rock, were carried out by M. Revering [24] to study the expected angular distribution of cosmic muons ProANUBIS should see. Figure 21 shows angular distributions of reconstructed tracks, with at least three RPCs hit, compared with the result of Geant4 simulations. All tracks were reconstructed pointing down ProANUBIS, with no timing information used for direction determination. Data from when the LHC beam was off on 01/03/24 was used for this reconstruction.

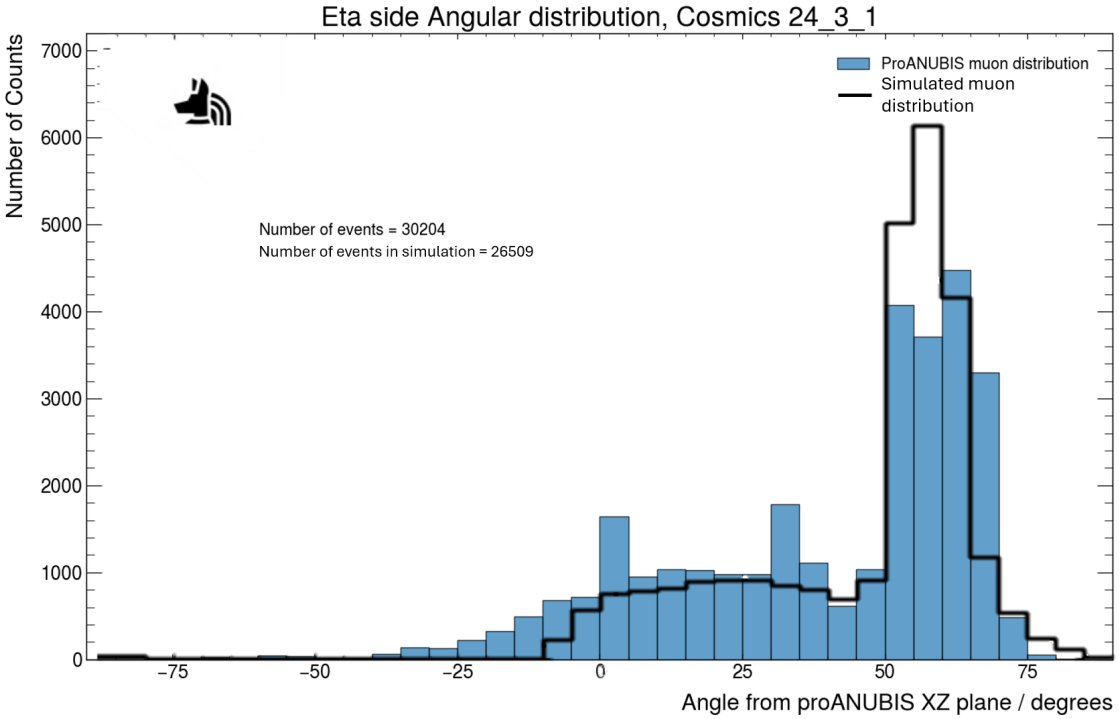

(a)

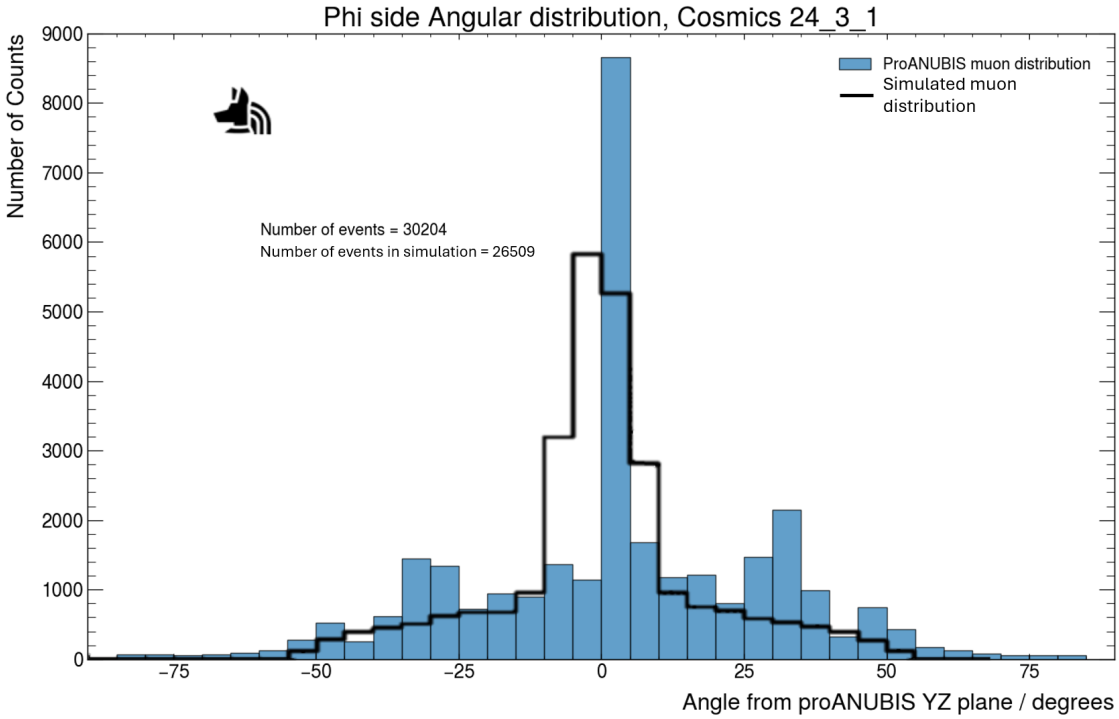

(b)

Figure 21: (a) Eta side and (b) phi side angular distribution for cosmic ray muons seen by ProANUBIS over three hours. The expected distribution for a similar number of events from M. Revering's simulation is shown in black.

The reconstructed events show good agreement with the Geant4 simulations, particularly picking up the large number of muons at 60° from the XZ plane due to the shaft entrance in the ATLAS cavern. The Geant4 simulation doesn't consider the discrete nature of the RPC strips, which have a width of 30mm (Appendix E) and are responsible for spikes in number of reconstructed events at angle bins such as 0°, 30° and 65° from the XZ plane. This

discreteness also causes the large peak at 0° and tail peaks at ± 30° and ± 50° from the YZ plane (Appendix E). The simulated result assumes the RPCs have 100% efficiency. The RPCs have lower efficiencies than this (Section 4.5), and do not have the same efficiencies, which will bias the angles further.

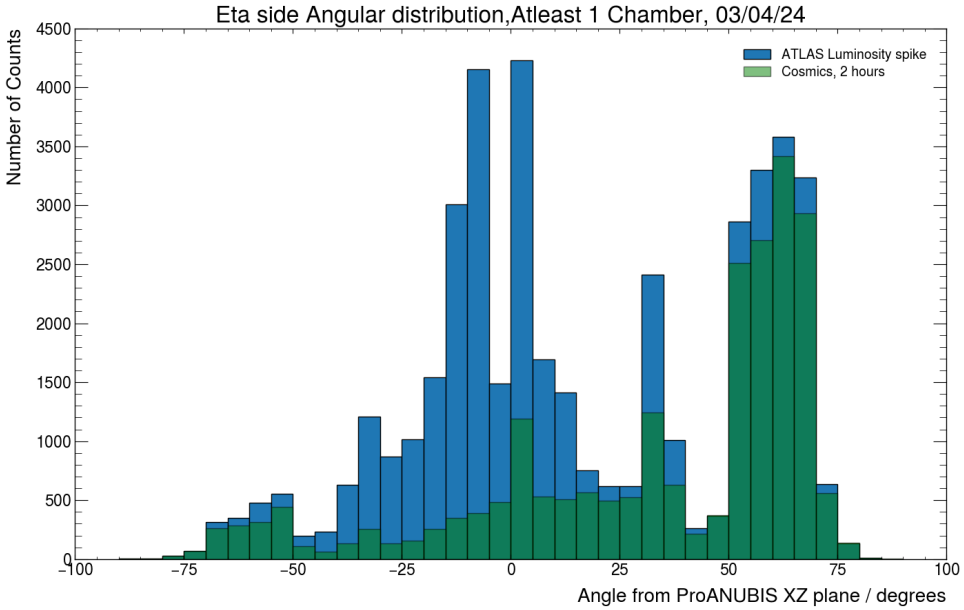

(a)

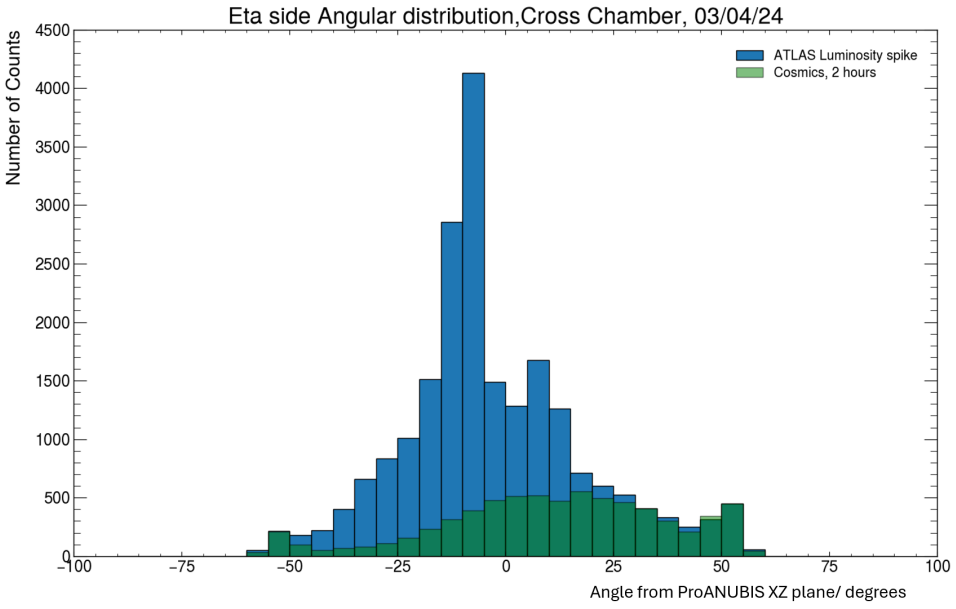

(b)

Figure 22: Eta side angular distribution while the LHC beam was on (blue) and off (green). (a) Has no restriction on number of chambers whereas (b) only reconstructs cross-chamber events.

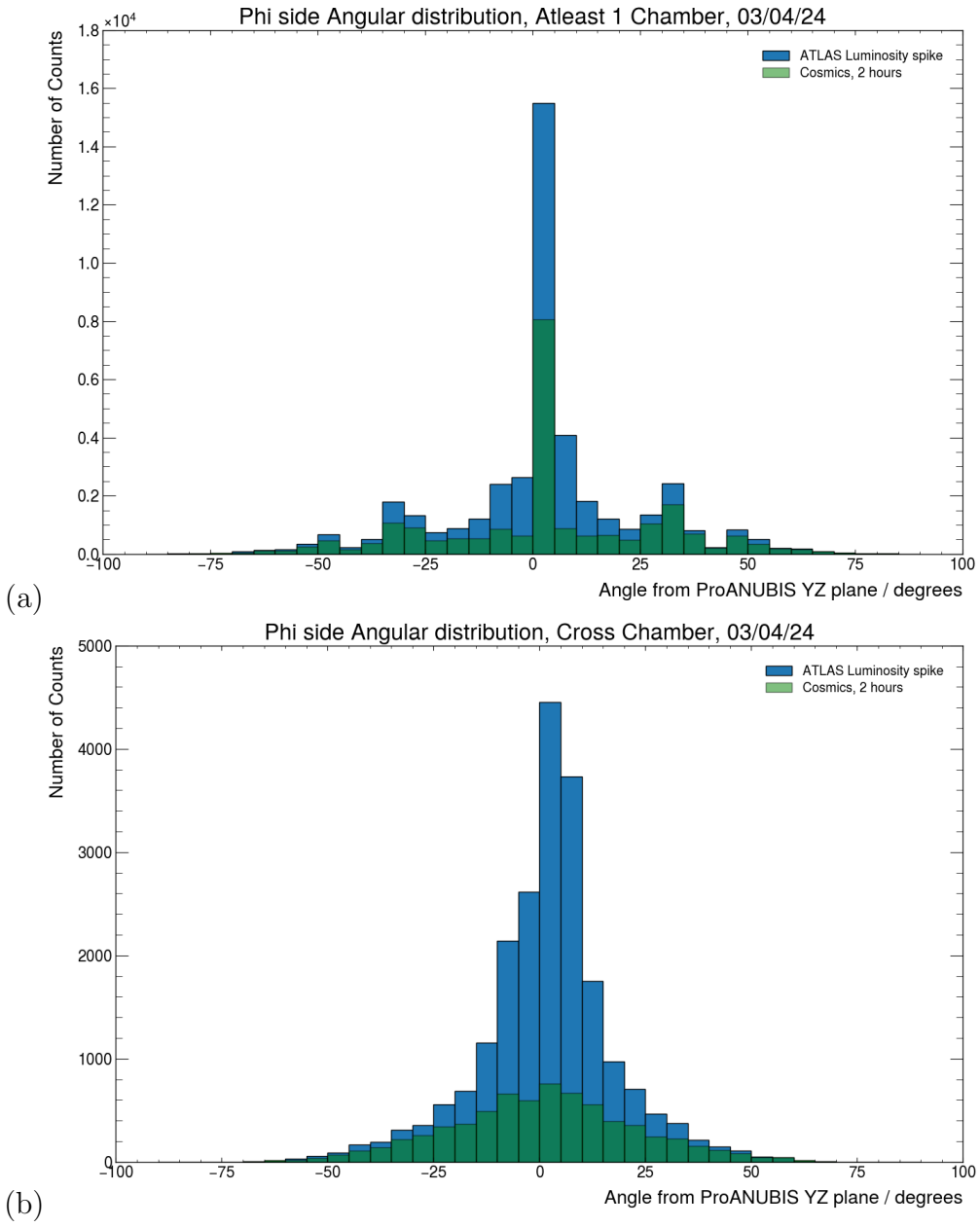

Figure 23: Same as Figure 22 but for the phi side.

Figures 22(a) and 23(a) show the eta and phi angular distributions for tracks reconstructed from at least three RPC hits with timing information taken into account, both for a two-hour period with the LHC beam on and off. An excess of events is seen when the LHC beam is on, showing ProANUBIS has sensitivity to particles produced in ATLAS. Introducing a cross-chamber constraint on reconstructed tracks cuts-off events with angles greater than 60° from the XZ plane. This effect is due to the geometry of the ProANUBIS setup, as most cosmic muons pass through the triplet layer only. This cross-chamber constraint is a geometrical filter for the cosmic background. The peak in excess events, when the LHC beam was on, at +10° from the XZ plane may originate from wrong direction determination by trajectory timing. The slight asymmetry in phi angular distribution suggests that ProANUBIS is slightly offset from the ATLAS interaction point.

4.5 Efficiencies

The SC setup discussed in Section 3 can be used for probing RPCs in a lab environment, but it is necessary to know the effects that operating in the ATLAS cavern has on RPC technology.

To probe an RPC's efficiency in-situ, firstly the test RPC is excluded from reconstructions. Tracks are reconstructed, with a 15 ns adaptive time window and max cluster size of three, using all five other RPCs in ProANUBIS. By requiring all five other RPCs to be present in the reconstruction, it is more likely the reconstructed track corresponds to a real particle and also less likely that the test RPC was involved in triggering the event read-out. This reduces the bias effect of using triggered data for efficiency measurements. If the reconstructed track passes through the test RPC, it is checked if the test RPC produces a usable coordinate within some distance tolerance of the expected hit location. Uncertainties were estimated for a 95% confidence interval, the same as in the SC efficiency measurement (Appendix C.2).

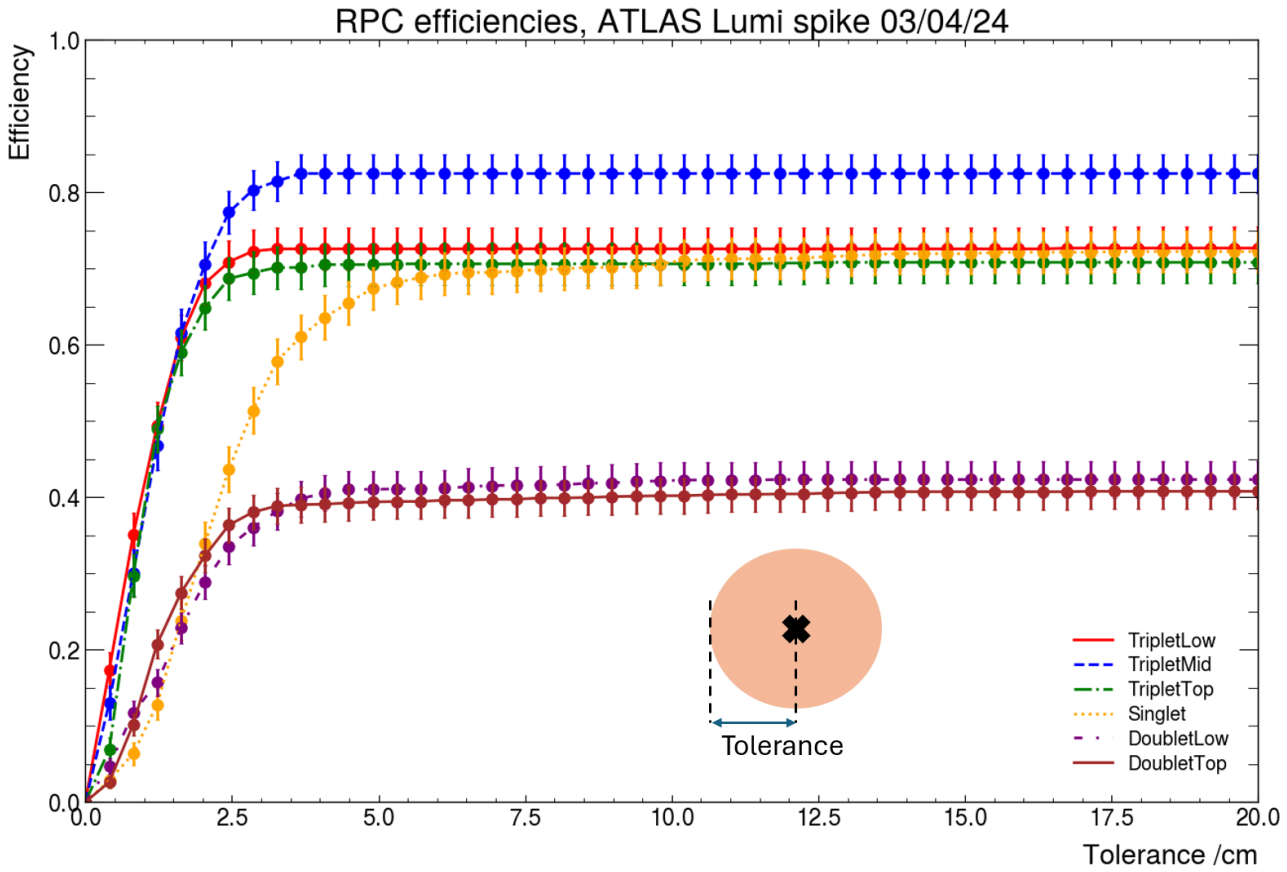

Figure 24: In-situ efficiency measurements of ProANUBIS RPCs during LHC Beam testing on 03/04/24.

The RPC efficiencies plateau (Figure 24) at values lower than would be required by RPCs in ANUBIS to reliably detect rare events associated with BSM LLP decays [6]. The lowest RPC efficiency measured was 40.8±2.3%, in the "Doublet Top" RPC. The later onset of the singlet and doublet plateaus compared to the triplet may be explained by the greater weighting of the triplet RPCs in track reconstruction, an artifact of the multiplet arrangement. A repeat measurement (Appendix F) on the same day with the LHC beam off produces consistent results, suggesting the low efficiency wasn't related to the on-state of the LHC beam.

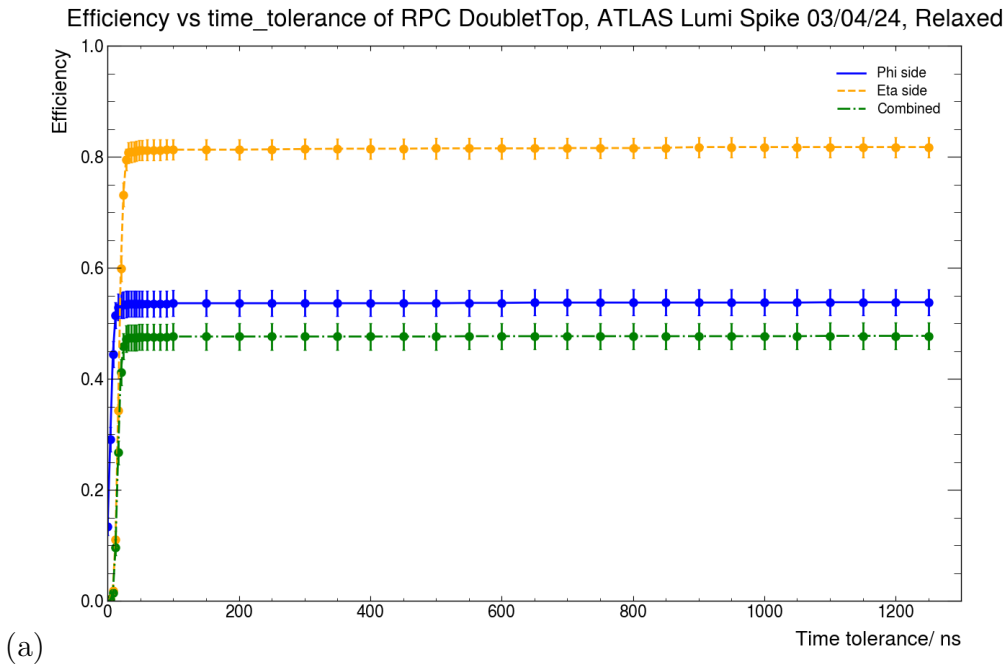

(a)

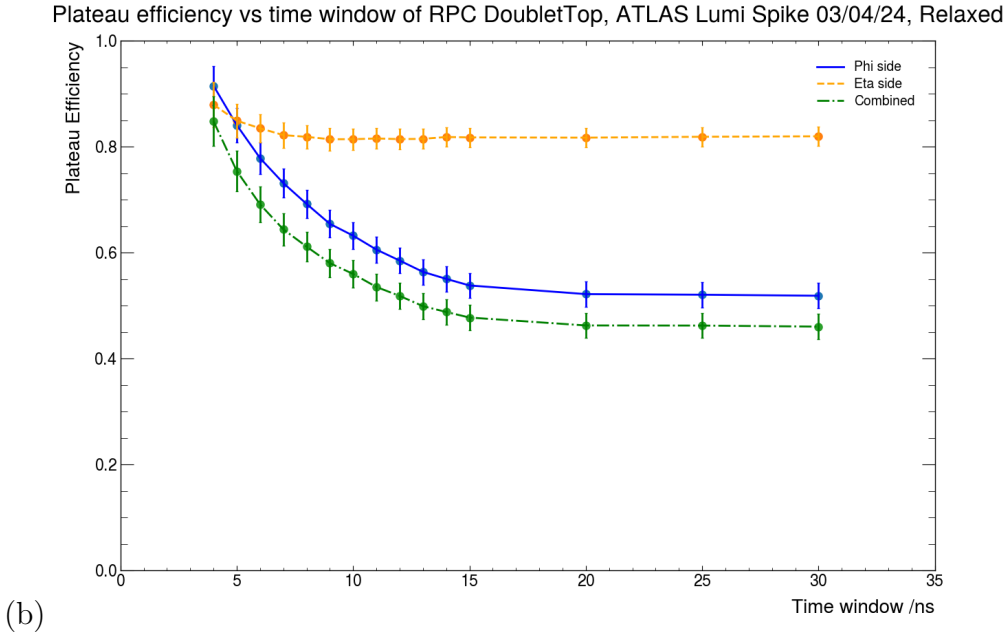

(b)

Figure 25: (a) In-situ efficiency scan for doublet top RPC. Phi, eta and their combination are probed separately. The same plots for other RPCs can be found in Appendix F. (b) A scan of the plateau efficiency, defined as the relaxed efficiency at 1250 ns time tolerance, with changing reconstruction time window.

A more relaxed probe of the RPCs was carried out to explore if the low efficiencies were an artifact of the reconstruction algorithm. All constraints on max cluster size and hit location in the test RPC were dropped. Instead, a temporal tolerance was introduced. The test RPC is asked to measure a hit in any channel within a time-frame around the time of a reconstructed event. Eta and phi channels were probed separately, with an example result for the "Doublet Top" RPC shown in Figure 25(a). The difference in eta and phi efficiencies for the same RPC implies a failure in the DAQ and/or FEB electronics. Both eta and phi plateau within 15-30 ns of the event time for most RPCs, indicating a low level of dark counts in the 1.25 µs trigger

window. Furthermore, Figure 25(a) shows the time-walk effect in eta strips, as the eta plateau is delayed by 15 ns with respect to the phi plateau. Figure 25(b) shows the plateau efficiency as a function of the time window used for reconstruction. Smaller time windows bias towards events closer to the FEBs, where the time-walk for signals is less, allowing for phi and eta hits to be clustered together. The increasing phi efficiency for smaller time windows may be explained by the phi strips closer to the eta FEBs being more efficient. An inspection of the TDC chips and FEB electronics of ProANUBIS may be necessary.

Current in-situ efficiency measurements of the ProANUBIS RPCs uses data whose readout is triggered by the RPCs, artificially increasing the measured efficiency of the RPC. When ProANUBIS is synced with the ATLAS clock, muons produced by collision in ATLAS can be tagged by ATLAS and used to probe the ANUBIS detectors with no bias, similar to "Tag and Probe" methods [25].

5 Conclusions

The scintillation counter setup in the ATLAS project room was upgraded with new electronics and SiPM mounts. A trigger threshold voltage of 720 mV for the scintillation counters was determined to give an optimum compromise between minimising both dark count rates and location and energy bias of triggered particles. The efficiencies of the upgraded scintillation counters were measured to be 93.9±0.8%, 97.2±0.9% and 95.0±0.9% at a threshold voltage of 720 mV, a reproducible result when comparator calibration is performed. Threshold scans of the scintillation counters' efficiencies show that an OR logic configuration is preferred over an AND logic to minimise location bias of particles.

A reconstruction algorithm was developed to investigate events in ProANUBIS. Tracks were reconstructed by minimising normalised χ^2 of trajectories fitted using SVD. The sensitivity of the reconstruction algorithm's results to the normalised χ^2-cutoff should be investigated. Reconstructed tracks of cosmic ray muon events had angular distributions that showed good agreement with Geant4 simulations, outside of the discrete nature of the RPCs strips. ProANUBIS was shown to have sensitivity to particles produced in ATLAS. The hit timings of events were investigated to see if ProANUBIS could distinguish between muons from cosmic rays and particles from interactions in ATLAS. The current algorithm sometimes misidentifies trajectory directions due to poor timing calibration. To improve, the finite time of signal propagation down read-out strips should be investigated. A new metric for defining the hit time of a cluster, such as earliest hit time, should be explored. A method for in-situ testing of RPC efficiency was developed which minimised bias when using data from triggered readouts. This highlighted potential problems with the FEB electronics and DAQ system of ProANUBIS.

Appendices

A Cosmic rays

An incident high energy cosmic ray, such as a proton, collides with nuclei in the upper atmosphere to create a variety of particles, but predominantly creating pions. The charged pions decay through the channel shown in Figure 26 (a) to produce muons and muon-neutrinos.

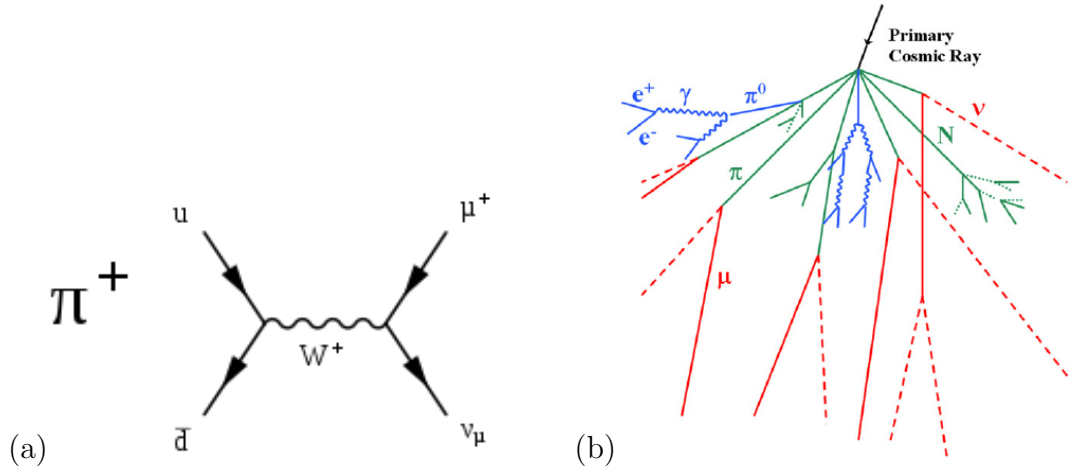

Figure 26: (a) Decay channel of charged pion resulting in muons, the branching ratio for muons is much larger than that for electrons since the muon's right-handed helicity state has a larger left-handed chiral component than the right-handed helicity electron. (b) Typical cosmic ray shower evolution, showing coupled hadronic and EM showers, image from [26].

At sea level, muons are the most numerous particle that originates from interactions of comsic rays in the upper-atmosphere. The electrons produced lose a large share of their energy to bremsstrahlung radiation [12]. The muons arrive at the Earth's surface with an average energy of 4 GeV at a flux of 1 cm^{-2} min^{-1} (integrated over solid angles of the upper hemisphere) for horizontal detectors [12]. The arrival rate of muons on a horizontal detector can be treated as a Poisson process with a mean flux of 1 cm^{-2} min^{-1}. Their average energy means that cosmic muons at the Earth's surface are minimally ionising and their average energy deposition rate with distance ($< -\frac{dE}{dx} >$) can be modelled by the Bethe-Bloch formula (Figure 27).

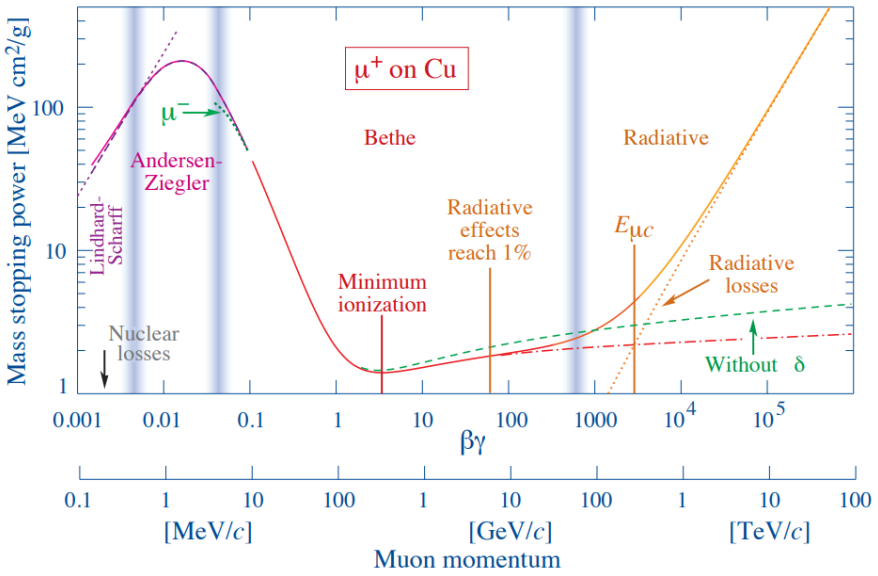

Figure 27: Variation of $< -\frac{dE}{dx} >$, normalised with density, with $\beta\gamma$ for anti-muons in copper. The Bethe-Bloch formula is valid for $\beta\gamma$ values of 1-1000. Other models describe the rest of the plot. Muons at the Earth's from cosmic ray origin are in the minimally ionising region. Image from [27].

A cosmic ray of sufficient energy can trigger an "air shower", a large correlated flux of particles at the Earth's surface. The shower consists of a hadronic core where neutral pions quickly decay through an electromagnetic interaction to produce photons which go on to cause EM sub-showers through pair production of electrons and positrons (Figure 26(b)).

B Initial setup tests

Threshold voltage scans of the dark count rates (DCR) of the initial setup's SiPMs were performed. The results in Figure 28(a) show that SiPMs four and seven have a step structure in a threshold scan, with each step corresponding to changing the number of photoelectrons in a pulse by one. Dark counts were assumed to occur independently and modelled as a Poisson process. The number of counts (N) were assumed to have errors (σ_N) due to shot noise (Equation (4)). The measurement of time (T) by the software had a resolution of 1 ms (σ_T). The errors for frequency measured are then found using Equation (3).

$$\frac{\sigma_f}{f} = \sqrt{(\frac{\sigma_N}{N})^2 + (\frac{\sigma_T}{T})^2} \tag{3}$$

Where,

$$\sigma_N = \sqrt{N} \tag{4}$$

To minimise shot noise, at least 1000 counts are collected per measurement. SiPMs nine and six show an absence of steps in their threshold scan, and large amounts of electrical noise in their signal, shown in Figure 28b. Similar issues were found with the setup by previous students [16]. The drop in hit rate for threshold voltages above 770 mV is due to saturation of electronics by dark-counts.

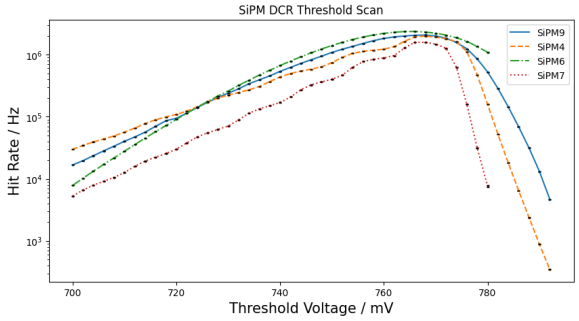

(a)

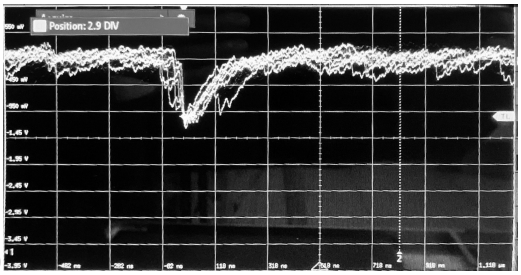

(b)

Figure 28: (a) Threshold scan of SiPM DCR when placed in dark bag. (b) Oscilloscope trace of output from SiPM nine. No band structure is observed.

A scan of the RV across the SiPM PN junctions was performed to determine the best operating VBIAS voltage. A potentiometer was used to change the RV applied across the PN junction inside SiPM nine. DCR of SiPM nine was measured with varying RV, with the threshold voltage kept at 760 mV to give a peak count rate. A breakdown voltage of 26.95±0.15 V, shown in 29, was measured. This value is in better agreement with Broadcom's stated breakdown voltage value of 26.9 V [14], when compared with previous students' results [16]. Increasing the RV to more than 6 V above the breakdown voltage causes increased DCR with diminishing increases in the PDE of the SiPM [14]. It was concluded that a RV of 30-32 V, supplied by the VBIAS generator, was a good compromise between increasing PDE and decreasing DCR.

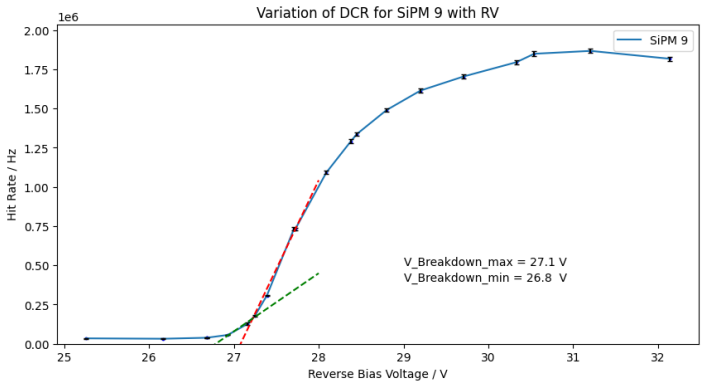

Figure 29: Hit rate VBIAS scan for SiPM nine at 760 mV threshold voltage, the voltage for peak response.

C Scintillation Counter calibration and reproducibility

C.1 Calibration

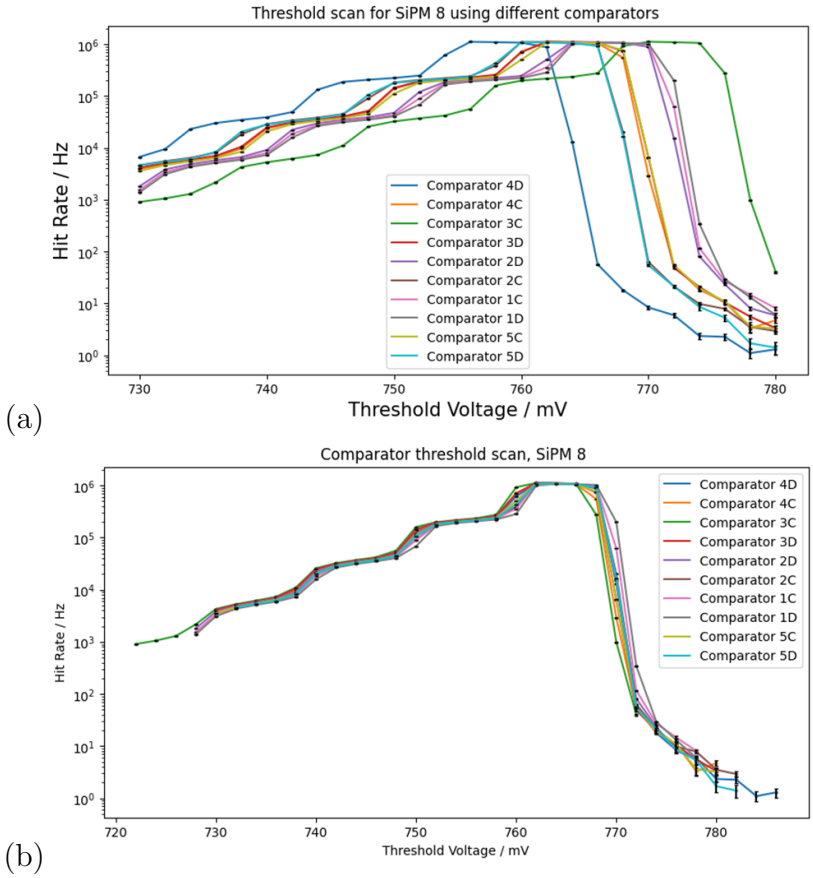

Figure 30: Threshold scan for SiPM eight with (b) and without (a) calibrating for comparator offsets.

Threshold scans of SiPM eight were used to calibrate the different comparator channel threshold voltages (Figure 30). Channels 3D, 4C and 5C were chosen to be the zero offset channels. The offsets are summarised in Table 1.

Comparator	Offset/mV
1 ChC	+2
1 ChD	+2
2 ChC	-2
2 ChD	+2
3 ChC	+8
3 ChD	0
4 ChC	0
4 ChD	-6
5 ChC	0
5 ChD	-2

Table 1: Offset values for comparator threshold voltages.

Any offset in the FPGA channels was checked by doing a threshold scan of SiPMs 8‖14 with comparator 5. No offset was observed (Figure 31).

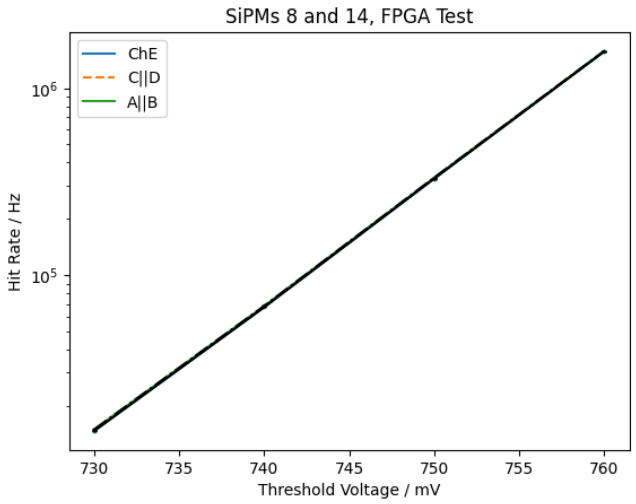

Figure 31: Measurement of SiPMs 8‖14 with different channels on the FPGA board.

C.2 Efficiency measurement uncertainties

The following equation was used to estimate the 95% confidence interval (CI) in efficiency measurements of the scintillation counters:

$$95\%CI \; = \; \eta \pm 1.96\sqrt{\frac{\eta(1-\eta)}{n}} \tag{5}$$

η is the measured efficiency. n is the number of trials. In this experiment n is the number of particles detected by the trigger, hence the number of possible particles that could be detected by the detector under test.

This corresponds to the binomial confidence interval of the true efficiency. It works well for intermediate efficiencies and large sample sizes. However, for efficiencies of 0 or 1 the formula predicts the measured efficiency has absolute certainty of being the true efficiency [28].

C.3 Reproducibility

Taking into account the comparator offsets, the efficiency measurements of the scintillation counters were found to be reproducible after a few days (Figure 32).

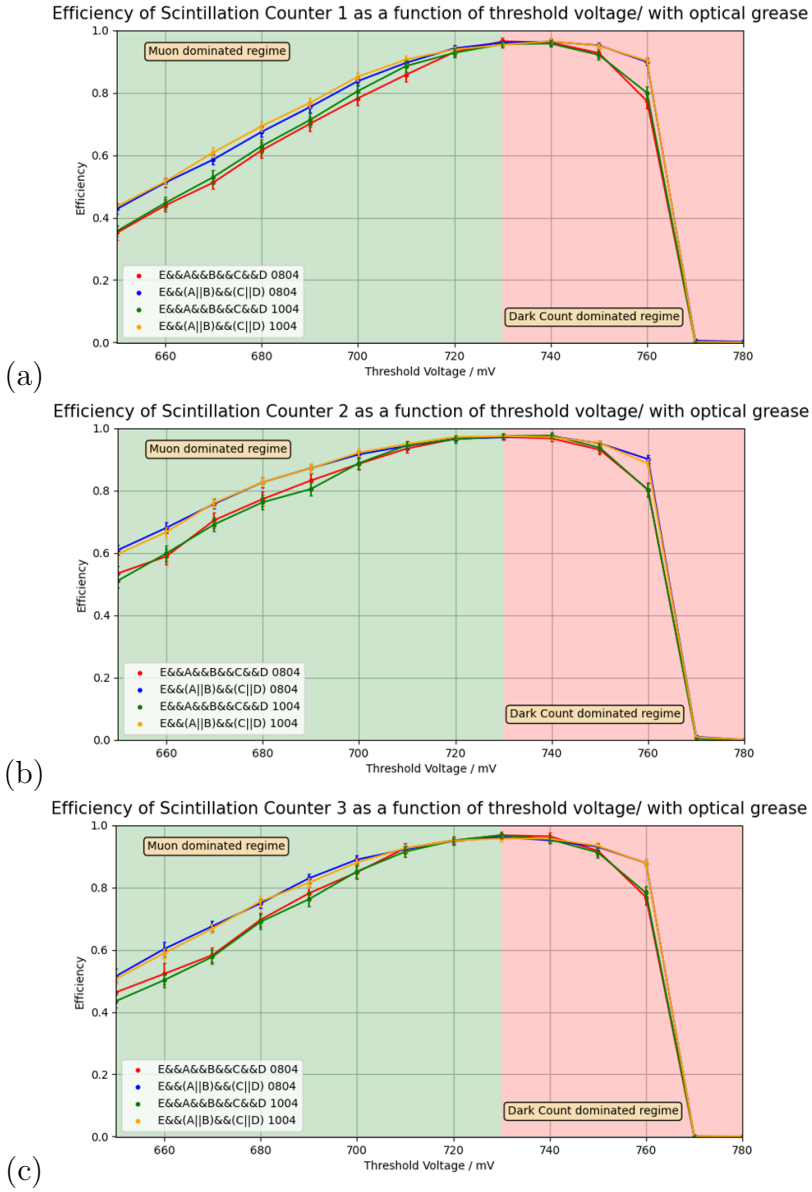

Figure 32: Reproducibility of scintillation counter efficiency measurements two days apart for SC 1 (a), SC 2 (b) and SC 3 (c).

D Track reconstruction algorithm

The data read out from a ProANUBIS trigger includes the information of which channels were hit in which RPC and at what time in the trigger window. Reconstruction algorithm:

1. First the data is clustered temporally using an adaptive time window. A time cluster is defined as a group of hits that hit within a time window of each other. The upper time window updates every time a new hit is added to a cluster, illustrated in Figure 33 with the time window set to 15 ns. This is done to filter out noise, which is assumed to happen stochastically at uncorrelated times.

Hit-time /ns	Action
250	First time in cluster registered as 250ns
254	254 ns – 250 ns = 4 ns < 15 ns Add this hit to the cluster, set cluster time to 254 ns.
260	260 ns – 254 ns = 6 ns < 15 ns Add this hit to the cluster, set cluster time to 260 ns.
276	276 ns – 260 ns = 16 ns > 15 ns This hit lies outside the time window. The cluster is complete, and a new cluster is defined with a start time of 276 ns.
...	...

Figure 33: Example of the time clustering method with a time window of 15 ns set.

2. The temporally clustered data then undergoes spatial clustering. A cluster is defined as defined as a continuous block of adjacent channels that fire.

3. (x,y) coordinates are extracted from the mid-points of eta and phi clusters respectively. If a cluster size is above the max cluster size set by the user, no coordinates are extracted from that cluster. The errors (σ_i) are estimated to originate from a uniform distribution over a single strip width. The z-coordinate of the RPC gives the z coordinate of the hit, this is assumed to have negligible error compared to the x and y errors.

4. Events can then be filtered based on:
   a. Minimum number of RPCs.
   b. Minimum number of Chambers.

5. This procedure can result in lots of (x,y) pairs for each RPC. Each possible combination of (x,y,z) sets of coordinates, with one coordinate per RPC, is generated.

6. SVD is used to fit a straight line [22] through each possible combination. The χ^2 value, normalised with respect to the number of degrees of freedom (N_{DOF}), is calculated for each fitted track using Equation (5).

$$\chi^2 = \frac{1}{N_{DOF}} \sum_{i=1}^{N} \frac{(O_i - E_i)^2}{\sigma_i} \tag{6}$$

   N is the number of reconstructed coordinates. O_i is the value of the observed coordinate and E_i is the expected value of the coordinate from the track constructed using SVD.

   N_{DOF} is estimated to be N subtract four, since there are two fitting parameters for the lines in the x and y directions each.

7. The reconstructed track that has the minimum normalised χ^2 value is chosen as the "real" particle track.

E Angular distributions and detector granularity

E.1 Angles

The reconstructed tracks were projected onto the XZ and YZ faces of the ProANUBIS setup (Figure 34). The dot product between the projected vectors and a unit vector parallel to the z direction then gave the desired angles (Figure 35).

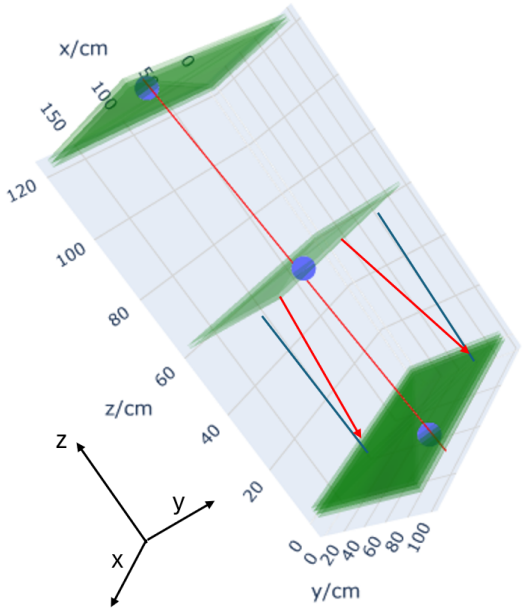

Figure 34: The reconstructed track, shown in red, is projected on to the side faces of the ProANUBIS setup.

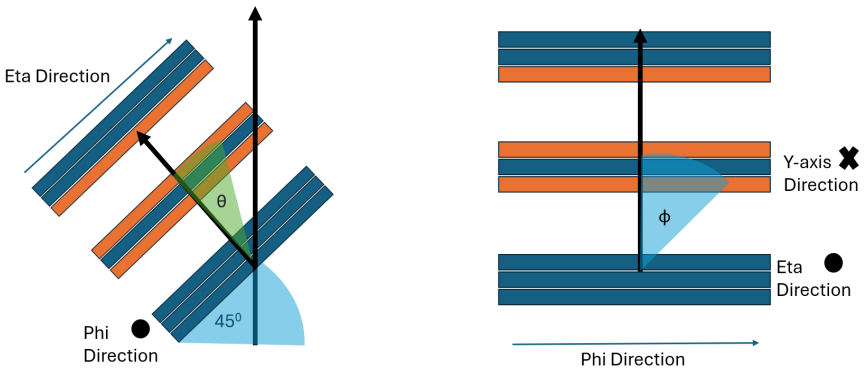

Figure 35: Cross-sections of ProANUBIS. (a) θ defines the angle from the XZ plane. (b) ϕ defines the angle from the YZ plane.

E.2 χ^2 distributions

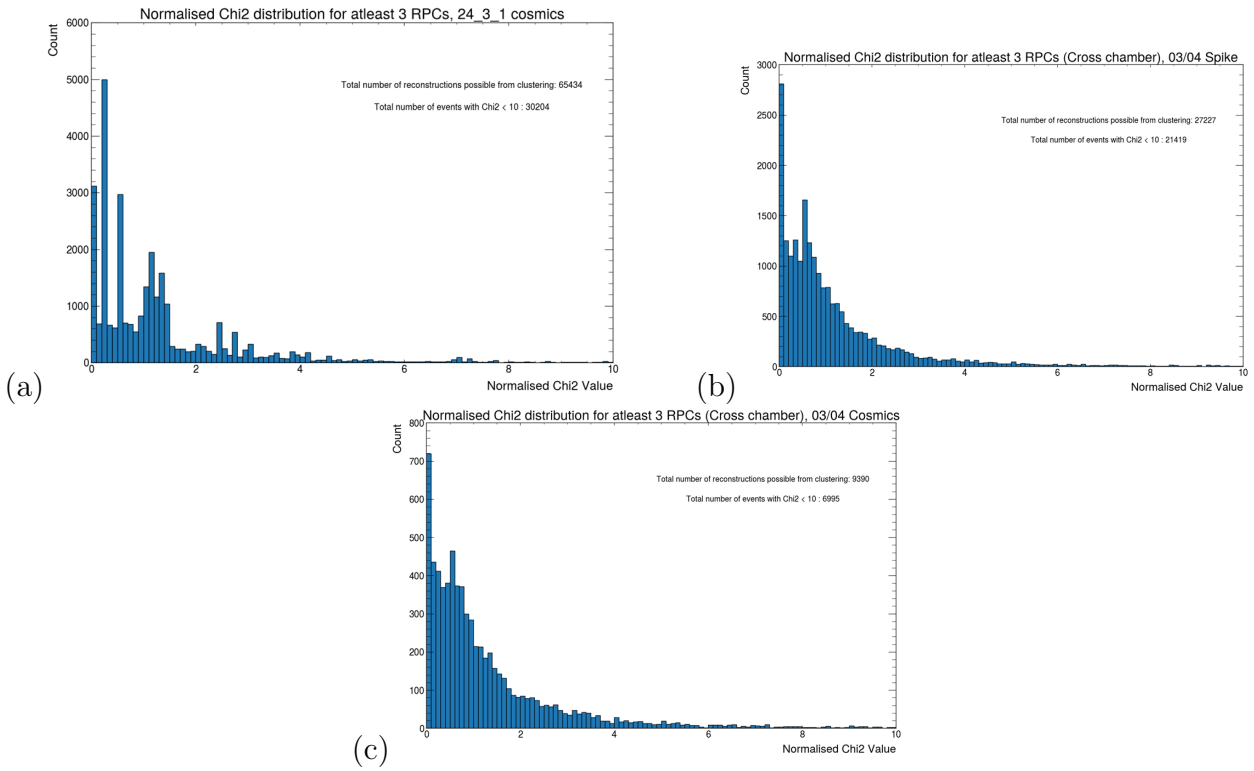

Figure 36: χ^2 distributions for reconstructed events: (a) Cosmics 01/03/24, (b) LHC beam on 03/04/24, (c) LHC beam off 03/04/24.

Figure 36 shows the normalised χ^2 distributions for reconstructed events used for finding angular distributions. The spikes in χ^2 seen in 36(a) are an artifact of the detector geometry, as discussed in Section 4.4, since no cross-chamber constraint is enforced.

E.3 Detector granularity

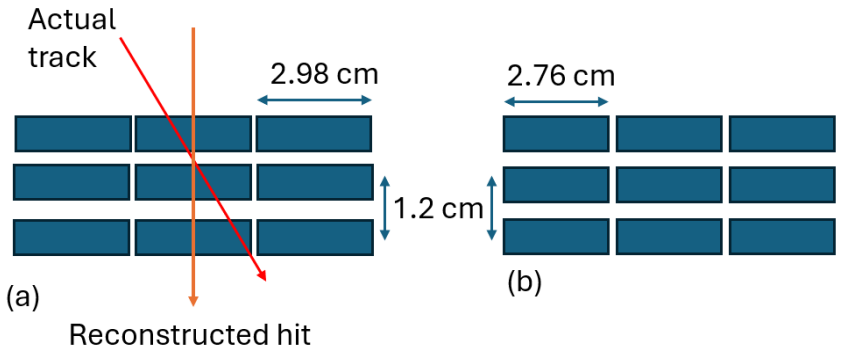

Figure 37: RPC triplet setup for (a) eta channels and (b) phi channels. The discrete nature of the RPC strips biases reconstructed tracks towards certain angles, as shown in the figure.

dY/cm	dZ/cm	Angle from XZ plane (°)
0.0	2.4	0.0
1.49	2.4	31.8
2.98	2.4	51.2
4.47	2.4	61.7
5.96	2.4	68.1

Table 2: Angles from XZ plane reconstructed if the travel in the eta direction (dY) is half-integer multiples of the eta-strip width. dZ is the travel along the axis perpendicular to the RPC planes.

dX/cm	dZ/cm	Angle from YZ plane (°)
0.0	2.4	0.0
1.38	2.4	29.90
2.76	2.4	49.0
5.52	2.4	61.7

Table 3: Angles from YZ plane reconstructed if the travel in the phi direction (dX) is half-integer multiples of the phi-strip width.

F ProANUBIS RPC efficiency measurements

Figure 38 shows the repeat measurement of ProANUBIS RPCs' efficiencies on 03/04/24 with varying spatial tolerance, this time with the LHC beam was switched off. The results are consistent with efficiencies for when the LHC beam was on 24.

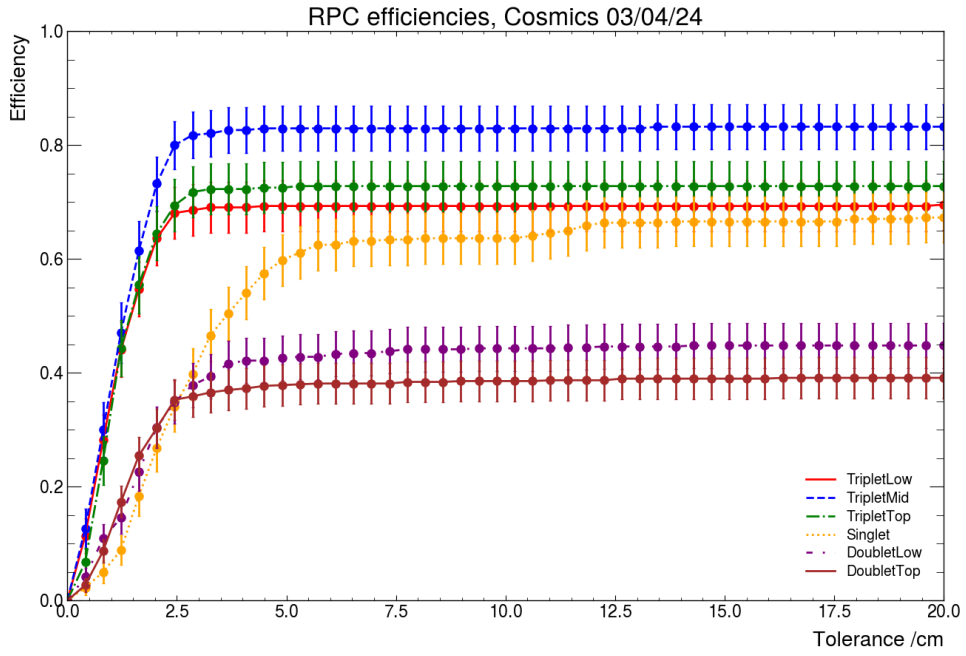

Figure 38: Efficiency scan with spatial tolerance for ProANUBIS RPCs on 03/04/24 with the LHC beam switched off.

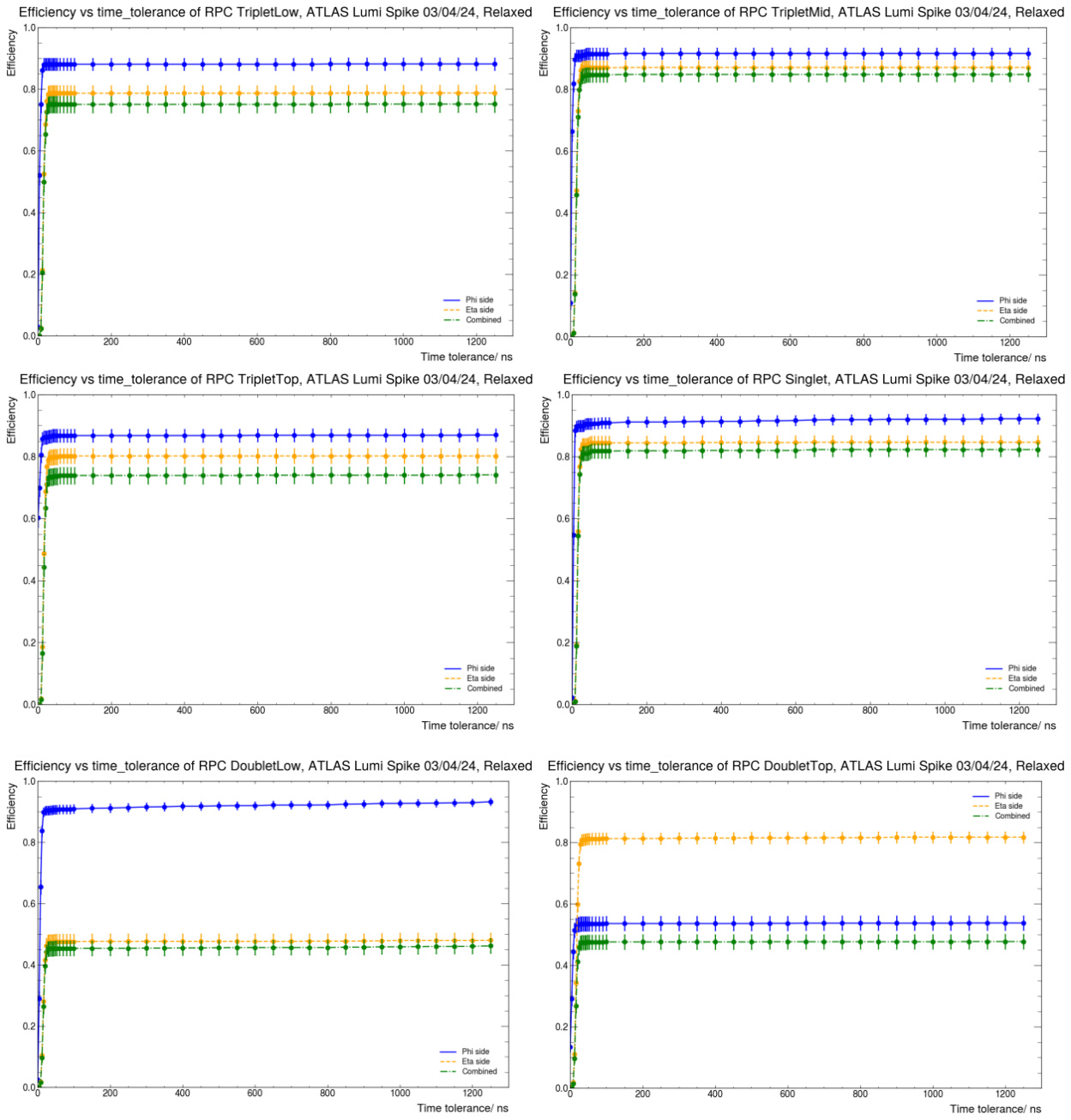

Figure 39: Relaxed efficiency scans for all six RPCs in ProANUBIS.

Source code

The code I developed for the track reconstruction of events in ProANUBIS is hosted publicly on my GitHub repository. This GitHub repository contains all my workings on how I developed each investigation of the ProANUBIS side of this report.

References

[1] Atlas Collaboration et al. "Observation of a new particle in the search for the Standard Model Higgs boson with the ATLAS detector at the LHC". *arXiv preprint arXiv:1207.7214* (2012).

[2] Douglas Clowe et al. "A Direct Empirical Proof of the Existence of Dark Matter*". *The Astrophysical Journal* 648.2 (2006), p. L109. DOI: 10.1086/508162. URL: https://dx.doi.org/10.1086/508162.

[3] Jonathan L Feng. "Dark matter candidates from particle physics and methods of detection". *Annual Review of Astronomy and Astrophysics* 48 (2010), pp. 495–545.

[4] Lawrence Lee et al. "Collider searches for long-lived particles beyond the Standard Model". *Progress in Particle and Nuclear Physics* 106 (2019), pp. 210–255. ISSN: 0146-6410. DOI: https://doi.org/10.1016/j.ppnp.2019.02.006. URL: https://www.sciencedirect.com/science/article/pii/S0146641019300109.

[5] Juliette Alimena et al. "Searching for long-lived particles beyond the Standard Model at the Large Hadron Collider". *Journal of Physics G: Nuclear and Particle Physics* 47.9 (2020), p. 090501.

[6] Martin Bauer et al. "ANUBIS: Proposal to search for long-lived neutral particles in CERN service shafts". *arXiv preprint arXiv:1909.13022* (2019).

[7] Alpigiani et al. "Recent progress and next steps for the MATHUSLA LLP detector". *arXiv preprint arXiv:2203.08126* (2022).

[8] "ANUBIS: a guide into the dark sector". *EP, Newsletter of the EP Department* (2023).

[9] Zhong He. "Review of the Shockley–Ramo theorem and its application in semiconductor gamma-ray detectors". *Nuclear Instruments and Methods in Physics Research Section A: Accelerators, Spectrometers, Detectors and Associated Equipment* 463.1-2 (2001), pp. 250–267.

[10] Ahmad Moshaii et al. "RPC simulation in avalanche and streamer modes using transport equations for electrons andions". *Nuclear Instruments and Methods in Physics Research Section A: Accelerators, Spectrometers, Detectors and Associated Equipment* 661 (2012), S168–S171.

[11] T. Reymermier. "Timing coincidence trigger setup". *Cavendish Laboratory, University of Cambridge* (2022).

[12] Particle Data Group, R L Workman, and et. al. "Review of Particle Physics". *Progress of Theoretical and Experimental Physics* 2022.8 (Aug. 2022), pp. 520–530. ISSN: 2050-3911. DOI: 10.1093/ptep/ptac097. eprint: https://academic.oup.com/ptep/article-pdf/2022/8/083C01/49175539/ptac097.pdf. URL: https://doi.org/10.1093/ptep/ptac097.

[13] "General Purpose Plastic Scintillator EJ-200, EJ-204, EJ-208, EJ-212". *Eljen Technology* (Jul 2021).

[14] "AFBR-S4N33C013, NUV-HD Single Silicon Photo Multiplier". *Broadcom* (Jan 2022).

[15] "Introduction to SiPM, Technical Note". *sensL* (2011).

[16] Yoshioka M., Liang W., and Atwal A. "RPC Project Report". *Cavendish Laboratory, University of Cambridge* (2023).

[17] Aashaq Shah. "Installation of proANUBIS–a proof-of-concept demonstrator for the ANUBIS experiment". *arXiv preprint arXiv:2401.09914* (2024).

[18] Thomas Peabody Satterthwaite. "Sensitivity of the ANUBIS and ATLAS Detectors to Neutral Long-Lived Particles Produced in *pp* Collisions at the Large Hadron Collider" (2022).

[19] Jon Burr. "Simulation Studies into the main backgrounds for ANUBIS". In: *Searching for long-lived particles at the LHC and beyond: Eleventh Workshop of the LLP Community*. University of Cambridge, Cavendish Laboratory. 2022.

[20] Ian Tomalin. "b tagging in CMS". In: *Journal of Physics: Conference Series*. Vol. 110. 9. IOP Publishing. 2008, p. 092033.

[21] Pierre Astier et al. "Kalman filter track fits and track breakpoint analysis". *Nuclear Instruments and Methods in Physics Research Section A: Accelerators, Spectrometers, Detectors and Associated Equipment* 450.1 (2000), pp. 138–154.

[22] Jonathon Shlens. "A tutorial on principal component analysis". *arXiv preprint arXiv:1404.1100* (2014).

[23] Giordano Cattani et al. "The Resistive Plate Chambers of the ATLAS experiment: performance studies". In: *Journal of Physics: Conference Series*. Vol. 280. 1. IOP Publishing. 2011, p. 012001.

[24] Michael Revering. "ProANUBIS Cosmic Flux simulation" (2024).

[25] Junghwan Goh et al. "CMS RPC efficiency measurement using the tag-and-probe method". *Journal of Instrumentation* 14.10 (2019), p. C10020.

[26] Francesco Blanco, Paola La Rocca, and Francesco Riggi. "Cosmic rays with portable Geiger counters: from sea level to airplane cruise altitudes". *European Journal of Physics* 30.4 (2009), p. 685. DOI: 10.1088/0143-0807/30/4/003. URL: https://dx.doi.org/10.1088/0143-0807/30/4/003.

[27] Donald E Groom and SR Klein. "Passage of particles through matter". *The European Physical Journal C-Particles and Fields* 15.1-4 (2000), pp. 163–173.

[28] Marc Paterno. "Calculating efficiencies and their uncertainties" (2004).